

Semi-implicit characteristic-based boundary treatment for acoustics in low Mach number flows

Yann Moguen, Erik Dick, Pascal Bruel

▶ **To cite this version:**

Yann Moguen, Erik Dick, Pascal Bruel. Semi-implicit characteristic-based boundary treatment for acoustics in low Mach number flows. Journal of Computational Physics, 2013, 255, pp.339 - 361. 10.1016/j.jcp.2013.08.019 . hal-02359072

HAL Id: hal-02359072

https://univ-pau.hal.science/hal-02359072

Submitted on 13 Nov 2019

HAL is a multi-disciplinary open access archive for the deposit and dissemination of scientific research documents, whether they are published or not. The documents may come from teaching and research institutions in France or abroad, or from public or private research centers.

L'archive ouverte pluridisciplinaire **HAL**, est destinée au dépôt et à la diffusion de documents scientifiques de niveau recherche, publiés ou non, émanant des établissements d'enseignement et de recherche français ou étrangers, des laboratoires publics ou privés.

*Manuscript
Click here to view linked References

Semi-implicit characteristic-based boundary treatment for acoustics in low Mach number flows

Yann Moguen [a], Pascal Bruel [b,*] and Erik Dick [a]

[a] *Ghent University – Department of Flow, Heat and Combustion Mechanics, Sint-Pietersnieuwstraat, 41 – 9 000 Gent, Belgium.*

[b] *CNRS, Université de Pau et des Pays de l'Adour LMAP UMR 5142 and Inria CAGIRE Team – Avenue de l'Université – 64 013 Pau, France*

Abstract

For low Mach number flow calculation, when acoustic waves have to be captured, semi-implicit methods allow to avoid the time-step limitation that arises when explicit schemes are used. A method is suggested to solve the boundary equations so that the semi-implicitness of the algorithm is maintained, as well as its pressure-velocity coupling. This method is studied theoretically and numerically, in the low Mach number regime. Partially non-reflective characteristic-based boundary conditions, with the linear relaxation form suggested by Rudy and Strikwerda, [*J. Comput. Phys.* 36:55–70, 1980], are considered. It is shown that their properties, well known in the framework of explicit schemes, are recovered with the proposed semi-implicit treatment and an acoustic CFL number significantly larger than unity.

Key words: Characteristic-based boundary conditions, Low Mach number flow, Semi-implicit algorithm, Acoustics

1 Introduction

For low Mach number flow calculations that include the capture of acoustic waves propagating in the flow, semi-implicit methods allow to avoid the time-step limitation that arises when explicit schemes are used. Then, it is of particular importance to maintain the semi-implicitness of the algorithm when solving the boundary equations. Among the variety of artificial boundary techniques (see Colonius [1]), characteristic-based boundary conditions, as suggested by Thompson [19] and

* Corresponding author. Tel.: +33 5 59 40 75 52.
Email address: pascal.bruel@univ-pau.fr (Pascal Bruel).

Poinsot and Lele [12], are widely used. An important advantage of such an approach is that the computational domain does not have to be much larger than the flow region of interest. Therefore, the computational cost is not drastically increased by the boundary treatment. Despite the important amount of studies on characteristic-based boundary conditions, according to the authors' knowledge, no investigation of the semi-implicit solution of characteristic-based boundary equations in SIMPLE-type algorithms has been published [1]. The aim of the present paper is to provide a detailed description of an effective semi-implicit solution of characteristic-based boundary equations.

In addition to computational cost considerations, the benefits of characteristic-based boundary conditions are recognized when acoustic waves have to be properly handled at the boundary (see Ref. [2]). For example, the specification of an incoming acoustic wave at the outlet can be carried out by handling the wave amplitudes in a straightforward manner, and this is not the case when a time-varying outflow pressure is simply imposed. Furthermore, the characteristic-based approach allows radiation of acoustic waves to the far field, *i.e.* transparent – or non-reflective – boundary conditions. This is suitable when the sound field is of interest, and avoids convergence problems caused by unphysical reflections. Let us underline that characteristic-based boundary conditions are not the only way to obtain transparency and to facilitate proper handling of acoustics at the boundary (see *e.g.* Refs. [3,16], where a buffer zone approach combined with a characteristic analysis allows also both the proper handling of boundary quantities and the damping of outgoing acoustic waves). The present study is focused only on the class of characteristic-based methods for the boundary conditions.

As a first approach of such characteristic-based treatment, the linear relaxation form of the non-reflective condition, suggested by Rudy and Strikwerda [15], is employed in the present study. It can be understood as a weakening of the crude full non-reflective condition, which consists in setting to zero the temporal rate of change of the entering acoustic wave amplitude. The linear relaxation method represents a trade-off between the imposition of variables and the partial reflection of acoustic waves. This is carried out by filtering the entering acoustic waves, so that only the high frequency band is concerned with the non-reflective treatment. Selle *et al.* [17] established that the relaxation coefficient is proportional to the highest frequency of the acoustic waves sent back into the computational domain. Therefore, the smaller the gap between the current and the imposed pressures, the larger the band of the reflected acoustic waves at the outlet. Following this approach, the linear relaxation must be applied to the pressure at the outlet, which behaves as a low-pass filter for the reflected waves. In particular, the direct imposition of the static pressure at the outlet is fully reflective for acoustic waves. Combined with the

[1] Some numerical simulations with a semi-implicit pressure correction method were presented in Ref. [20], but without information concerning the method employed for the semi-implicit boundary treatment.

time evolution equations of the primitive variables of the flow (see Refs. [12,19]), the relaxation form appears suitable to avoid the drift of the pressure which may arise if the full non-reflective conditions are applied. The allowed reflection of low frequency waves permits to relate the pressure variable inside the domain to the static pressure defined outside, thus ensuring the well-posedness of the problem (see *e.g.* [12] for details on well-posedness). Similar results concern the velocity at the inlet of the computational domain.

This paper is organized as follows. First, the algorithmic framework used, which consists in a SIMPLE-type algorithm in co-located arrangement with second-order accuracy in time and space, is described in section 2. A focus on the pressure-velocity coupling involved in the interior of the computational domain was found necessary since the boundary treatment is designed in such a way that this pressure-velocity coupling is accounted for therein. Then, in section 3, characteristic-based boundary conditions with the linear relaxation approach employed by Rudy and Strikwerda [15] are presented. An expression for the relaxation coefficient of the velocity at the inlet is suggested. The semi-implicit solution of the characteristic-based boundary conditions is detailed in section 4. Both the inlet and the outlet treatments are considered. Finally, in section 5, the capability of this boundary treatment is investigated by considering 1-D and 2-D test cases with linear acoustic waves propagating in low Mach number flows.

The key point of the suggested approach is the derivation from the momentum and velocity equations of a relation between pressure and velocity corrections at the boundary, that mimics the SIMPLE approximation used in the interior of the computational domain. This relation, together with the conservation equations and the equations satisfied by the temporal rate of change of the wave amplitudes, written in the interior and at the boundary of the computational domain, respectively, allows the calculation of the pressure and velocity corrections on the boundary cells.

2 Algorithm for the interior of the computational domain

In this section, the pressure correction algorithm for the interior of the computational domain is presented. In Ref. [10], we described a more general formulation of such predictor-corrector algorithm. A simplified version of this formulation is adopted in the present contribution, with the same results for the set of computations considered. A step-by-step presentation of the algorithm is given here. For explanations on the theoretical background of the used algorithm, the reader is referred to [10]. In the present section, it will be worth describing with details the pressure-velocity coupling aspects in the basic algorithm, since they are mimicked by the proposed treatment of the boundary equations explained in section 4.

For sake of simplicity, a one-dimensional flow of a perfect and ideal gas in a con-

stant section pipe is considered. From now on, x denotes the coordinate in the flow direction. The flow is governed by the Euler equations,

$$\partial_t \varrho + \partial_x(\varrho v) = 0, \tag{1a}$$
$$\partial_t(\varrho v) + \partial_x(\varrho v^2 + p) = 0, \tag{1b}$$
$$\partial_t(\varrho E) + \partial_x(\varrho v H) = 0, \tag{1c}$$
$$E = e + \frac{1}{2}v^2, \;\; \varrho H = \varrho E + p, \;\; \varrho e = \frac{p}{\gamma - 1}, \tag{1d}$$

where t, ϱ, p, v, e, E and H represent time, density, pressure, velocity, internal energy, total energy and total enthalpy per unit mass, respectively. Furthermore, γ denotes the specific heats ratio. The x axis along the pipe is divided into N cells of length Δx. A finite volume formulation is applied, with co-located variables at the centres of the cells.

The solution procedure is in classic prediction-correction form. Each time-step $n \to n+1$ is decomposed into a predictor step determining variables at an intermediate level denoted by $\star$, followed by a corrector step with correction quantities denoted by $\prime$. Furthermore, since the equations are non-linear, iterations denoted by k are used in between the time levels n and $n+1$. At the first iteration, variables at level k are equal to those at time level n. The velocity written with subscript $i+1/2$ is the transporting velocity. The velocity as a transported quantity is part of the transported momentum and is defined with a slope-limiter method.

• ***Prediction***. Predicted values are derived from the continuity equation (1a) and the momentum equation (1b). For example, the momentum equation is written as

$$\begin{aligned}
&\frac{1}{2\tau}\left[3(\varrho v)_i^\star - 4(\varrho v)_i^n + (\varrho v)_i^{n-1}\right] \\
&+ \left\{(\varrho v)_i^\star + \frac{1}{2}\psi_i\left((\varrho v)^k\right)\left[(\varrho v)_i^k - (\varrho v)_{i-1}^k\right]\right\} v_{i+1/2}^k \\
&- \left\{(\varrho v)_{i-1}^\star + \frac{1}{2}\psi_{i-1}\left((\varrho v)^k\right)\left[(\varrho v)_{i-1}^k - (\varrho v)_{i-2}^k\right]\right\} v_{i-1/2}^k \\
&\qquad\qquad + p_{i+1/2}^k - p_{i-1/2}^k = 0.
\end{aligned} \tag{2}$$

The face value of pressure is taken through the low Mach number adaptation of AUSM$^+$ [7], with the scaling function of the AUSM$^+$-up scheme [8], but without the velocity diffusion term in the pressure interpolation formula and without the pressure dissipation term in the definition of the Mach number at the face [10]. This means that the face pressure is determined by a polynomial interpolation between values on both sides of the face, obtained from the definition:

$$p_{i+1/2} = f_p^+(M_\mathrm{L})p_\mathrm{L} + f_p^-(M_\mathrm{R})p_\mathrm{R}, \tag{3}$$

where the polynomials f_p^+ and f_p^- are function of the Mach number on both sides, and where the face values are obtained by means of the slope-limiter method. The

face value of the velocity $v^k_{i+1/2}$ is calculated through the AUSM$^+$ scheme. The discretization of the continuity equation is similar as the one of the momentum equation. Thus, the time integration is second-order backward and the space discretization is second-order TVD, by means of the limiter function denoted by ψ. The parameter τ stands formally for $\Delta t/\Delta x$ and is determined in practice by $\mathrm{CFL}_v/v_{\max}$, where CFL_v denotes a chosen convective CFL number and $v_{\max}$ is the maximum value of the convective velocity in the field. The convective terms in Eq. (2) and in the discretized continuity equation are assumed to be positive, as they are positive in the computations considered later.

From the predicted values of density $\varrho^\star_i$ and momentum $(\varrho v)^\star_i$, predicted values of velocity $v^\star_i$ are determined at the nodes. Combined with $p^\star = p^k$, predicted values $e^\star_i$, $E^\star_i$ and $(\varrho H)^\star_i$ are obtained according to Eqs. (1d). Next, predicted values of the face pressure $p^\star_{i+1/2}$ are calculated with the same procedure as for $p^k_{i+1/2}$. To calculate predicted values of face velocity $v^\star_{i+1/2}$, the Momentum Interpolation technique is used. It is based on the observation that the momentum equation (2) at a node is of the form

$$B_i = A_i(\varrho v)^\star_i + \frac{1}{2\tau}\Big[3(\varrho v)^\star_i - 4(\varrho v)^n_i + (\varrho v)^{n-1}_i\Big] + p^k_{i+1/2} - p^k_{i-1/2},$$

with

$$B_i = -\left\{\frac{1}{2}\psi_i\left((\varrho v)^k\right)\left[(\varrho v)^k_i - (\varrho v)^k_{i-1}\right]\right\}v^k_{i+1/2} + \left\{(\varrho v)^\star_{i-1} + \frac{1}{2}\psi_{i-1}\left((\varrho v)^k\right)\left[(\varrho v)^k_{i-1} - (\varrho v)^k_{i-2}\right]\right\}v^k_{i-1/2}$$

and $A_i = v^k_{i+1/2}$. A similar equation is postulated at a face as

$$B_{i+1/2} = A_{i+1/2}(\varrho v)^\star_{i+1/2} + \frac{1}{2\tau}\Big[3(\varrho v)^\star_{i+1/2} - 4(\varrho v)^n_{i+1/2} + (\varrho v)^{n-1}_{i+1/2}\Big] + p^k_{i+1} - p^k_i,$$

where two terms in the balance of the momentum fluxes are interpolated, but where the inertia term and the pressure term are written directly at the face. The so-called classic Rhie-Chow interpolation is used, namely:

$$\frac{2}{A_{i+1/2}} = \frac{1}{A_i} + \frac{1}{A_{i+1}}, \qquad \frac{B_{i+1/2}}{A_{i+1/2}} = \frac{B_i}{A_i} + \frac{B_{i+1}}{A_{i+1}}.$$

The precise way of interpolation is in fact not critical, provided that the linear interpolation involves convective terms only, without a part of the inertia term [6,10,11]. The transporting face velocity is deduced from the momentum equation by

$$v^\star_{i+1/2} = (\varrho v)^\star_{i+1/2} \Big/ \varrho^\star_{i+1/2},$$

where the face density is defined with the slope-limiter method.

• ***Correction***. As regards pressure-velocity coupling, a critical point of the algorithm is the relation between pressure corrections and velocity corrections. Following the SIMPLE approximation, an explicit relation between momentum corrections and pressure corrections can then be obtained from the momentum equation, as

$$\left(v^k_{i+1/2} + \frac{3}{2\tau}\right)(\varrho v)'_i = -(p'_{i+1/2} - p'_{i-1/2}), \tag{4}$$

or else, in a even further simplified form which is chosen in the present algorithm,

$$\left(v^k_i + \frac{3}{2\tau}\right)(\varrho v)'_i = -(p'_{i+1/2} - p'_{i-1/2}). \tag{5}$$

Considering the smallness of the time-step that has been used in the cases considered in the present study, numerical results with Eq. (4) and Eq. (5), or else, by approximating the left hand side of Eq. (5) by $3(\varrho v)'_i/(2\tau)$, are in fact found to be identical. Thus, the exact form of the SIMPLE approximation adopted in the present study appears to be not critical. In Eq. (5), $p'_{i+1/2}$ and $p'_{i-1/2}$ are interpolated with the AUSM$^+$-up polynomials (see Eq. (3)), as

$$p'_{i+1/2} = f^+_p(M^\star_i)p'_i + f^-_p(M^\star_{i+1})p'_{i+1}.$$

Corrections for pressure are derived from the energy equation. This equation is discretized in the same style as the continuity equation and the momentum equation by

$$\begin{aligned}
&\frac{1}{2\tau}\left[3(\varrho E)^\star_i + 3(\varrho E)'_i - 4(\varrho E)^n_i + (\varrho E)^{n-1}_i\right] \\
&+ \left\{(\varrho H)^\star_i + \frac{1}{2}\psi_i\left((\varrho H)^\star\right)\left[(\varrho H)^\star_i - (\varrho H)^\star_{i-1}\right]\right\} v^\star_{i+1/2} \\
&- \left\{(\varrho H)^\star_{i-1} + \frac{1}{2}\psi_{i-1}\left((\varrho H)^\star\right)\left[(\varrho H)^\star_{i-1} - (\varrho H)^\star_{i-2}\right]\right\} v^\star_{i-1/2} \\
&\qquad + (\varrho H v)'_{i+1/2} - (\varrho H v)'_{i-1/2} = 0.
\end{aligned} \tag{6}$$

The corrections on the enthalpy flux terms are written as

$$(\varrho H v)'_{i+1/2} = H^\star_{i+1/2}(\varrho v)'_{i+1/2} + (\varrho H)'_{i+1/2} v^\star_{i+1/2}, \tag{7}$$

with $H^\star_{i+1/2} = (\varrho H)^\star_{i+1/2}/\varrho^\star_{i+1/2}$, where both terms in the ratio are defined with the slope-limiter method. The corrections for total energy and total enthalpy are written as

$$(\varrho E)'_i = \frac{1}{\gamma - 1}p'_i, \;\; (\varrho H)'_{i+1/2} = \frac{\gamma}{\gamma - 1}p'_{i+1/2}. \tag{8}$$

The momentum correction in Eq. (7) is written in SIMPLE-style, similarly to (5),

as

$$\left(v^{\star}_{i+1/2} + \frac{3}{2\tau}\right)(\varrho v)'_{i+1/2} = -(p'_{i+1} - p'_i). \tag{9}$$

Substitution of (8) and (9) into (7) and (6) leads to an extended Poisson equation for the pressure corrections, where, again, gradient terms are approximated to first-order. This equation is solved by a Gaussian elimination procedure. The pressure corrections are then further used to determine corrections of the momentum values in the nodes and at the faces by (5) and (9). Density is corrected by $\varrho'_i = (\partial_p \varrho)^{\star}_i p'_i$. The whole procedure is repeated until convergence. This results then in equations for mass, momentum and energy, discretized in the same way as the momentum equation (2), with values on the $\star-$level and $k-$level replaced by values on the time level $n+1$. All equations use the same value of the transporting velocity at the faces.

3 Characteristic-based boundary conditions: linear relaxation form

In this section, the temporal rate of change of the convective and acoustic wave amplitudes is introduced, as well as the linear relaxation form for the partially non-reflective treatment at the inlet and at the outlet. The justification of this approach at low Mach number is addressed in the Appendix section.

First, it is worth noticing that the following characteristic relations are derived from the set (1) of equations (see *e.g.* Thompson [19]),

$$\frac{\mathrm{d}p}{\varrho c} - \mathrm{d}v = 0 \quad \text{on} \quad \mathrm{d}_t x = v - c,$$

$$\mathrm{d}\varrho - \frac{1}{c^2}\mathrm{d}p = 0 \quad \text{on} \quad \mathrm{d}_t x = v,$$

$$\frac{\mathrm{d}p}{\varrho c} + \mathrm{d}v = 0 \quad \text{on} \quad \mathrm{d}_t x = v + c.$$

Then, let us set

$$\mathcal{L}_1 = (v - c)\left(\frac{1}{\varrho c}\partial_x p - \partial_x v\right), \tag{10a}$$

$$\mathcal{L}_2 = v\left(\partial_x \varrho - \frac{1}{c^2}\partial_x p\right), \tag{10b}$$

$$\mathcal{L}_3 = (v + c)\left(\frac{1}{\varrho c}\partial_x p + \partial_x v\right). \tag{10c}$$

The quantities $\mathcal{L}_i$, defined for $i = 1, 2, 3$ in 1-D, are interpreted as the temporal rate of change of the wave amplitudes at the boundary [12,13]. They satisfy the so-called LODI (for Locally One Dimensional and Inviscid) equations [12,19],

$$\partial_t \varrho + \frac{\varrho}{2c}(\mathcal{L}_1 + \mathcal{L}_3) + \mathcal{L}_2 = 0, \tag{11a}$$

$$\partial_t v + \frac{1}{2}(\mathcal{L}_3 - \mathcal{L}_1) = 0, \tag{11b}$$

$$\partial_t p + \frac{\varrho c}{2}(\mathcal{L}_1 + \mathcal{L}_3) = 0. \tag{11c}$$

Following Ref. [15], a linear relaxation form of the full non-reflective outlet condition $\mathcal{L}_1 = 0$ can be considered,

$$\mathcal{L}_1 = K_p\,(p - p^\dagger), \tag{12}$$

where $p^\dagger$ and p are the target and the current value of the pressure at the outlet, respectively. The relaxation coefficient K_p is related to the filtering level of outgoing acoustic waves (see Ref. [17]), so that $K_p \neq 0$ corresponds to an acoustically partially reflective outlet. By using Eq. (12), the reflection of high frequency outgoing acoustic waves can be avoided while maintaining a given value of the mean pressure.

Using Eq. (12) under the hypothesis of a constant target pressure, the reflection coefficient at the outlet is given by [17]:

$$R_{\text{outlet}}(\omega) = -\frac{1}{1 - \mathrm{i}\frac{2\omega}{\varrho c K_p}}. \tag{13}$$

Assuming that K_p is independent of the frequency, Selle *et al.* [17] derived its expression from a particular value of the frequency. They chose the frequency that corresponds to the largest acoustic wavelength obtainable in a duct of length L. Such a frequency, so-called cut-off frequency, was estimated as

$$f_{\text{cut-off}} = \frac{\omega_{\text{cut-off}}}{2\pi} = \frac{(1 - M_{\text{max}}^2)c_{\text{min}}}{4L},$$

where M_{max} and c_{min} designate the maximum Mach number and the minimum sound speed in the domain, respectively. Then, Selle *et al.* [17] required that half of the acoustic energy would be fed back into the domain for an acoustic wave of frequency $f_{\text{cut-off}}$ crossing the outlet section, *i.e.*:

$$|R_{\text{outlet}}(\omega_{\text{cut-off}})|^2 = 1/2. \tag{14}$$

Combination of relations (13) and (14) provides the expression of K_p:

$$K_p = \frac{\pi(1 - M_{\text{max}}^2)}{\varrho L}. \tag{15}$$

The role of the factor $1/2$ in the right hand side of Eq. (14) will be illustrated by numerical experiments in section 5, as well as in the similar equation suggested underneath for the inlet treatment.

Similarly as for the outlet, a linear relaxation of the full non-reflective condition $\mathcal{L}_3 = 0$ can be considered at the inlet, as

$$\mathcal{L}_3 = K_v(v - v^\dagger), \tag{16}$$

where $v^\dagger$ is the target velocity. To obtain a suitable expression of K_v, a frequency analysis similar to the one given in Ref. [17] yields [2]

$$R_{\text{inlet}}(\omega) = \frac{1}{1 - \mathrm{i}\frac{2\omega}{K_v}}. \tag{17}$$

Next, assuming that at the inlet section, the reflection coefficient is, again, such that $|R_{\text{inlet}}(\omega_{\text{cut-off}})|^2 = 1/2$, provides the expression of K_v, namely:

$$K_v = \frac{\pi(1 - M_{\max}^2)c_{\min}}{L}. \tag{18}$$

4 Semi-implicit treatment of the characteristic-based boundary conditions

In this section, a method to solve the boundary equations (11) with the relaxation forms given in section 3, in combination with the algorithm used in the interior of the computational domain, is described. It is achieved by introducing ghost cells at the inlet and at the outlet of the domain. In the one-dimensional case considered in this section, two ghost cells are introduced at each extremity of the domain, in order to use second-order accurate finite differences for the gradients. The ghost cells are numbered 1 and 2 at the inlet, and $N-1$ and N at the outlet. On these ghost cells, the primitive variables density, velocity and pressure, which are the unknowns of the LODI equations (11), are calculated following the prediction-correction procedure used for the interior solution. This allows to relate predicted and correction values on ghost cells to predicted and correction values of the interior solution, respectively, in order to mimic the suitable pressure-velocity coupling used in the interior algorithm.

[2] Expression (17) of the reflection coefficient at the inlet was also considered in Ref. [13].

4.1 Inlet treatment

At the inlet, the temporal rate of change of the amplitude of the entropic waves is written as

$$\mathcal{L}_2 = K_\varrho(\varrho - \varrho^\dagger), \tag{19}$$

where $\varrho^\dagger$ is the target inlet density and K_ϱ a relaxation coefficient. Furthermore, from Eq. (18),

$$\mathcal{L}_3 = \chi_{\text{in}}\frac{v - v^\dagger}{L} \quad , \quad \chi_{\text{in}} = \pi(1 - M_{\max}^2)c_{\min}, \tag{20}$$

where $v^\dagger$ is the target inlet velocity. Eqs. (19) and (20) are used on cells 1 and 2. Moreover, $\mathcal{L}_1$ is given by Eq. (10a).

• ***Prediction***. $\varrho_1^\star$ is calculated from the continuity equation (11a),

$$\begin{aligned}\frac{3\varrho_1^\star - 4\varrho_1^n + \varrho_1^{n-1}}{2\Delta t} + \left(\frac{\varrho}{2c}\right)_1^k \chi_{\text{in}}\frac{v_1^k - v^\dagger}{L} - \left(\frac{\varrho}{2c}\right)_1^k (v-c)_1^k \frac{-3v_1^k + 4v_2^k - v_3^k}{2\Delta x} \\ + \frac{(v-c)_1^k}{2(c_1^k)^2}\frac{-3p_1^k + 4p_2^k - p_3^k}{\Delta x} + K_\varrho(\varrho_1^\star - \varrho^\dagger) = 0\end{aligned} \tag{21}$$

$\varrho_2^\star$ is calculated similarly from the mass equation (11a) written on cell 2.

From the velocity equation (11b) written on cell 2,

$$\begin{aligned}\frac{3v_2^\star - 4v_2^n + v_2^{n-1}}{2\Delta t} + \frac{1}{2}(v-c)_2^k \frac{-3v_2^\star + 4v_3^\star - v_4^\star}{2\Delta x} \\ - \frac{1}{2}\left(\frac{v-c}{\varrho c}\right)_2^k \frac{-3p_2^k + 4p_3^k - p_4^k}{2\Delta x} + \frac{1}{2}\chi_{\text{in}}\frac{v_2^\star - v^\dagger}{L} = 0\end{aligned} \tag{22}$$

$v_3^\star$ and $v_4^\star$ are unknown at this stage. However, with the momentum equation (2) written on cells 3 and 4, a linear system is obtained, allowing to compute $v_2^\star$, $v_3^\star$ as well as $v_4^\star$. Then, knowing $v_2^\star$ and $v_3^\star$, $v_1^\star$ can be directly calculated from the velocity equation (11b) written on cell 1.

• ***Correction***. First, Eq. (5), which is valid for the cells located in the interior of the computational domain, is simplified to

$$(\varrho v)_i' = -\frac{2}{3}\tau(p'_{i+1/2} - p'_{i-1/2}). \tag{23}$$

This simplification is justified by the very small values of the convective CFL number that we will use in the numerical tests. On cell 3, the velocity correction is

deduced as

$$v_3' = -\frac{\Delta t}{3\varrho_3^\star \Delta x}(p_4' - p_2'), \tag{24}$$

where the pressure has been interpolated centrally (choice consistent with AUSM pressure interpolation at low Mach number). The velocity equation (11b) on cell 2 and on iteration level $k+1$, is

$$\frac{3v_2^{k+1} - 4v_2^n + v_2^{n-1}}{2\Delta t} + \frac{1}{2}(v-c)_2^k \frac{-3v_2^{k+1} + 4v_3^{k+1} - v_4^{k+1}}{2\Delta x} - \frac{1}{2}\left(\frac{v-c}{\varrho c}\right)_2^k \frac{-3p_2^{k+1} + 4p_3^{k+1} - p_4^{k+1}}{2\Delta x} + \frac{1}{2}\chi_{\text{in}}\frac{v_2^{k+1} - v^\dagger}{L} = 0 \tag{25}$$

From Eqs. (22) and (25), and considering the gradients at the first order accurate approximation, follows

$$\frac{3v_2'}{2\Delta t} + \frac{1}{2}(v-c)_2^k \frac{v_3' - v_2'}{\Delta x} - \frac{1}{2}\left(\frac{v-c}{\varrho c}\right)_2^k \frac{p_3' - p_2'}{\Delta x} + \frac{1}{2}\chi_{\text{in}}\frac{v_2'}{L} = 0. \tag{26}$$

Notice that the derivation of Eq. (26) from the velocity equation (11b) at the inlet, is similar to the derivation of Eq. (5) from the momentum equation in the interior of the computational domain. With Eq. (24), the velocity correction on cell 2 can be expressed as

$$v_2' = \mathcal{A}_2 p_2' + \mathcal{B}_2 p_3' + \mathcal{C}_2 p_4', \tag{27}$$

where

$$\begin{aligned}
\mathcal{A}_2 &= -\left[\frac{1}{2\Delta x}\left(\frac{v-c}{\varrho c}\right)_2^k + \frac{1}{2\Delta x}(v-c)_2^k \frac{\Delta t}{3\varrho_3^\star \Delta x}\right] \Big/ \mathcal{D}_2, \\
\mathcal{B}_2 &= \frac{1}{2\Delta x}\left(\frac{v-c}{\varrho c}\right)_2^k \Big/ \mathcal{D}_2, \\
\mathcal{C}_2 &= \frac{1}{2\Delta x}(v-c)_2^k \frac{\Delta t}{3\varrho_3^\star \Delta x} \Big/ \mathcal{D}_2, \\
\mathcal{D}_2 &= \frac{3}{2\Delta t} - \frac{1}{2\Delta x}(v-c)_2^k + \frac{\chi_{\text{in}}}{2L}.
\end{aligned} \tag{28}$$

The pressure equation (11c) on cell 2, is

$$\frac{3p_2^{k+1} - 4p_2^n + p_2^{n-1}}{2\Delta t} + \frac{1}{2}(\varrho c)_2^k \chi_{\text{in}} \frac{v_2^{k+1} - v^\dagger}{L} - \frac{1}{2}(\varrho c)_2^k (v-c)_2^k \frac{-3v_2^{k+1} + 4v_3^{k+1} - v_4^{k+1}}{2\Delta x} + \frac{1}{2}(v-c)_2^k \frac{-3p_2^{k+1} + 4p_3^{k+1} - p_4^{k+1}}{2\Delta x} = 0.$$

Then, with a first order approximation of the gradients of pressure and velocity corrections and using Eqs. (24) and (27), this becomes:

$$\alpha p_2' + \beta p_3' + \gamma p_4' = \delta, \tag{29}$$

where

$$\alpha = \frac{3}{2\Delta t} + \mathcal{A}_2 \left(\frac{1}{2}(\varrho c)_2^k \frac{\chi_{\text{in}}}{L} + \frac{1}{2\Delta x}(\varrho c)_2^k (v-c)_2^k \right) - \frac{1}{2\Delta x}(\varrho c)_2^k (v-c)_2^k \frac{\Delta t}{3\varrho_3^\star \Delta x} - \frac{1}{2\Delta x}(v-c)_2^k,$$

$$\beta = \mathcal{B}_2 \left(\frac{1}{2}(\varrho c)_2^k \frac{\chi_{\text{in}}}{L} + \frac{1}{2\Delta x}(\varrho c)_2^k (v-c)_2^k \right) + \frac{1}{2\Delta x}(v-c)_2^k,$$

$$\gamma = \mathcal{C}_2 \left(\frac{1}{2}(\varrho c)_2^k \frac{\chi_{\text{in}}}{L} + \frac{1}{2\Delta x}(\varrho c)_2^k (v-c)_2^k \right) + \frac{1}{2\Delta x}(\varrho c)_2^k (v-c)_2^k \frac{\Delta t}{3\varrho_3^\star \Delta x},$$

$$\delta = -\frac{3p_2^k - 4p_2^n + p_2^{n-1}}{2\Delta t} - \frac{1}{2}(\varrho c)_2^k \chi_{\text{in}} \frac{v_2^\star - v^\dagger}{L} + \frac{1}{2}(\varrho c)_2^k (v-c)_2^k \frac{-3v_2^\star + 4v_3^\star - v_4^\star}{2\Delta x} - \frac{1}{2}(v-c)_2^k \frac{-3p_2^k + 4p_3^k - p_4^k}{2\Delta x}. \tag{30}$$

The momentum is corrected on the second cell as

$$(\varrho v)_2^{k+1} = \varrho_2^\star \left(1 + \frac{p_2'}{p_2^k} \right) (v_2^\star + v_2'),$$

where $\varrho_2^\star$, $v_2^\star$ and v_2' are given by Eqs. (21), (22) and (27), respectively.

Now, let us describe how to calculate v_1' and p_1'. First, v_1' can be expressed with pressure corrections similar as was done previously for v_2', namely:

$$\mathcal{D}_1 v_1' = \mathcal{B}_1 (p_2' - p_1') - \frac{1}{2\Delta x}(v-c)_1^k v_2', \tag{31}$$

where

$$\mathcal{B}_1 = \frac{1}{2\Delta x} \left(\frac{v-c}{\varrho c} \right)_1^k \Big/ \mathcal{D}_1,$$

$$\mathcal{D}_1 = \frac{3}{2\Delta t} - \frac{1}{2\Delta x}(v-c)_1^k + \frac{\chi_{\text{in}}}{2L}.$$

A possibility for the expression of v_2' in Eq. (31) is to use Eq. (27), which would be consistent with the treatment of the cell 2. However, numerical experiments (not shown here) reveal that stability problems may occur with this choice. In this case, v_1' would depend on p_4', as well as p_1' to p_3'. This corresponds to a strong downwind treatment with respect to the flow direction. Alternatively, an expression of v_2' that

depends on p_1' and p_3' can be derived from the SIMPLE approximation, when the pressure at the face is interpolated centrally:

$$v_2' = -\frac{\Delta t}{3\varrho_2^\star \Delta x}(p_3' - p_1').$$

Then, the LODI velocity and pressure equations lead to relations involving v_1' and p_1', p_2' and p_3' quite similar to Eqs. (27)–(28) and Eqs. (29)–(30). The momentum on the cell 1 is corrected according to

$$(\varrho v)_1^{k+1} = \varrho_1^\star \left(1 + \frac{p_1'}{p_1^k}\right)(v_1^\star + v_1').$$

4.2 Outlet treatment

The outlet treatment described in section 3 is now considered, with the relaxation form given in Eqs. (12) and (15), rewritten for convenience as

$$\mathcal{L}_1 = \frac{\chi_{\text{out}}}{\varrho}\frac{p - p^\dagger}{L} \quad , \quad \chi_{\text{out}} = \pi(1 - M_{\max}^2).$$

This expression is used on cells $N-1$ and N.

• ***Prediction***. On cells $N-1$ and N, the predicted density and velocity are given by Eqs. (11a)-(11b). For instance, on cell $N-1$, the density is given by

$$\begin{aligned}
&\frac{3\varrho_{N-1}^\star - 4\varrho_{N-1}^n + \varrho_{N-1}^{n-1}}{2\Delta t} + \left(\frac{\varrho}{2c}\right)_{N-1}^k (v+c)_{N-1}^k \frac{3v_{N-1}^k - 4v_{N-2}^k + v_{N-3}^k}{2\Delta x} \\
&+ \left(\frac{v+c}{2c^2}\right)_{N-1}^k \frac{3p_{N-1}^k - 4p_{N-2}^k + p_{N-3}^k}{2\Delta x} + \left(\frac{1}{2c}\right)_{N-1}^k \chi_{\text{out}} \frac{p_{N-1}^k - p^\dagger}{L} \\
&+ v_{N-1}^k \frac{3\varrho_{N-1}^\star - 4\varrho_{N-2}^\star + \varrho_{N-3}^\star}{2\Delta x} - \left(\frac{v}{c^2}\right)_{N-1}^k \frac{3p_{N-1}^k - 4p_{N-2}^k + p_{N-3}^k}{2\Delta x} = 0
\end{aligned} \tag{32}$$

and the velocity is given by

$$\begin{aligned}
&\frac{3v_{N-1}^\star - 4v_{N-1}^n + v_{N-1}^{n-1}}{2\Delta t} - \frac{\chi_{\text{out}}}{2\varrho_{N-1}^k}\frac{p_{N-1}^k - p^\dagger}{L} \\
&+ \frac{1}{2}(v+c)_{N-1}^k \frac{3v_{N-1}^\star - 4v_{N-2}^\star + v_{N-3}^\star}{2\Delta x} \\
&\qquad + \frac{1}{2}\left(\frac{v+c}{\varrho c}\right)_{N-1}^k \frac{3p_{N-1}^k - 4p_{N-2}^k + p_{N-3}^k}{2\Delta x} = 0.
\end{aligned} \tag{33}$$

• ***Correction***. The pressure equation (11c), with implicit discretization for pressure and velocity reads on cell $N-1$:

$$\frac{3p_{N-1}^{k+1}-4p_{N-1}^{n}+p_{N-1}^{n-1}}{2\Delta t}+\frac{1}{2}(\varrho c)_{N-1}^{k}(v+c)_{N-1}^{k}\frac{3v_{N-1}^{k+1}-4v_{N-2}^{k+1}+v_{N-3}^{k+1}}{2\Delta x}$$
$$+\frac{1}{2}(v+c)_{N-1}^{k}\frac{3p_{N-1}^{k+1}-4p_{N-2}^{k+1}+p_{N-3}^{k+1}}{2\Delta x}+\frac{1}{2}c_{N-1}^{k}\chi_{\text{out}}\frac{p_{N-1}^{k+1}-p^{\dagger}}{L}=0. \quad (34)$$

Expressions of v'_{N-2} and v'_{N-1} in terms of pressure corrections are needed. First, since the cell $N-2$ belongs to the interior of the computational domain (see Eq. (23)),

$$(\varrho v)'_{N-2}=-\frac{2}{3}\tau(p'_{N-2+1/2}-p'_{N-2-1/2}).$$

With central interpolation for the pressure corrections,

$$v'_{N-2}=-\frac{\Delta t}{3\varrho^{\star}_{N-2}\Delta x}(p'_{N-1}-p'_{N-3}). \quad (35)$$

Second, the implicit discretization for pressure and velocity of Eq. (11b) reads:

$$\frac{3v_{N-1}^{k+1}-4v_{N-1}^{n}+v_{N-1}^{n-1}}{2\Delta t}-\frac{\chi_{\text{out}}}{2\varrho_{N-1}^{k}}\frac{p_{N-1}^{k+1}-p^{\dagger}}{L}$$
$$+\frac{1}{2}(v+c)_{N-1}^{k}\frac{3v_{N-1}^{k+1}-4v_{N-2}^{k+1}+v_{N-3}^{k+1}}{2\Delta x}$$
$$+\frac{1}{2}\left(\frac{v+c}{\varrho c}\right)_{N-1}^{k}\frac{3p_{N-1}^{k+1}-4p_{N-2}^{k+1}+p_{N-3}^{k+1}}{2\Delta x}=0. \quad (36)$$

From Eqs. (33), (35) and (36), with the gradients of corrections expressed in a first order accurate form,

$$v'_{N-1}=\mathcal{A}_{N-1}p'_{N-1}+\mathcal{B}_{N-1}p'_{N-2}+\mathcal{C}_{N-1}p'_{N-3}, \quad (37)$$

where

$$\mathcal{A}_{N-1}=\left[\frac{\chi_{\text{out}}}{2\varrho_{N-1}^{k}L}-\frac{1}{2\Delta x}\left(\frac{v+c}{\varrho c}\right)_{N-1}^{k}-\frac{1}{2\Delta x}(v+c)_{N-1}^{k}\frac{\Delta t}{3\varrho^{\star}_{N-2}\Delta x}\right]\Big/\mathcal{D}_{N-1},$$

$$\mathcal{B}_{N-1}=\left[\frac{1}{2\Delta x}\left(\frac{v+c}{\varrho c}\right)_{N-1}^{k}\right]\Big/\mathcal{D}_{N-1},$$

$$\mathcal{C}_{N-1}=\left[\frac{1}{2\Delta x}(v+c)_{N-1}^{k}\frac{\Delta t}{3\varrho^{\star}_{N-2}\Delta x}\right]\Big/\mathcal{D}_{N-1},$$

$$\mathcal{D}_{N-1}=\frac{3}{2\Delta t}+\frac{1}{2\Delta x}(v+c)_{N-1}^{k}.$$

The pressure equation (34) becomes finally, with the gradients of corrections expressed in a first order accurate form,

$$\alpha p'_{N-1} + \beta p'_{N-2} + \gamma p'_{N-3} = \delta,$$

where

$$\alpha = \frac{3}{2\Delta t} + \mathcal{A}_{N-1}\frac{1}{2\Delta x}(\varrho c)^k_{N-1}(v+c)^k_{N-1} + \frac{1}{2\Delta x}(\varrho c)^k_{N-1}(v+c)^k_{N-1}\frac{\Delta t}{3\varrho^\star_{N-2}\Delta x} + \frac{1}{2\Delta x}(v+c)^k_{N-1} + \frac{1}{2}c^k_{N-1}\frac{\chi_{\text{out}}}{L}$$

$$\beta = \mathcal{B}_{N-1}\frac{1}{2\Delta x}(\varrho c)^k_{N-1}(v+c)^k_{N-1} - \frac{1}{2\Delta x}(v+c)^k_{N-1}$$

$$\gamma = \mathcal{C}_{N-1}\frac{1}{2\Delta x}(\varrho c)^k_{N-1}(v+c)^k_{N-1} - \frac{1}{2\Delta x}(\varrho c)^k_{N-1}(v+c)^k_{N-1}\frac{\Delta t}{3\varrho^\star_{N-2}\Delta x}$$

$$\delta = -\frac{3p^k_{N-1} - 4p^n_{N-1} + p^{n-1}_{N-1}}{2\Delta t} - \frac{1}{2}(\varrho c)^k_{N-1}(v+c)^k_{N-1}\frac{3v^\star_{N-1} - 4v^\star_{N-2} + v^\star_{N-3}}{2\Delta x} - \frac{1}{2}(v+c)^k_{N-1}\frac{3p^k_{N-1} - 4p^k_{N-2} + p^k_{N-3}}{2\Delta x} - \frac{1}{2}c^k_{N-1}\chi_{\text{out}}\frac{p^k_{N-1} - p^\dagger}{L}.$$

The momentum on the cell $N-1$ is corrected according to

$$(\varrho v)^{k+1}_{N-1} = \varrho^\star_{N-1}\left(1 + \frac{p'_{N-1}}{p^k_{N-1}}\right)(v^\star_{N-1} + v'_{N-1}),$$

where $\varrho^\star_{N-1}$, $v^\star_{N-1}$ and v'_{N-1} are given by Eqs. (32), (33) and (37), respectively.

Similarly as for the derivation of v'_{N-1} given in Eq. (37), one has:

$$v'_N = \mathcal{A}_N p'_N + \mathcal{B}_N p'_{N-1} + \mathcal{C}_N v'_{N-1},$$

where

$$\mathcal{A}_N = \left[\frac{\chi_{\text{out}}}{2\varrho^k_N L} - \frac{1}{2\Delta x}\left(\frac{v+c}{\varrho c}\right)^k_N\right] \Big/ \mathcal{D}_N$$

$$\mathcal{B}_N = \left[\frac{1}{2\Delta x}\left(\frac{v+c}{\varrho c}\right)^k_N\right] \Big/ \mathcal{D}_N$$

$$\mathcal{C}_N = \frac{1}{2\Delta x}(v+c)^k_N \Big/ \mathcal{D}_N$$

$$\mathcal{D}_N = \frac{3}{2\Delta t} + \frac{1}{2\Delta x}(v+c)^k_N$$

Then, from the LODI pressure equation (similar to Eq. (34)) and from Eq. (37),

$$\lambda p'_N + \mu p'_{N-1} = \zeta,$$

where

$$\lambda = \frac{3}{2\Delta t} + \mathcal{A}_N \frac{1}{2\Delta x}(\varrho c)_N^k (v+c)_N^k + \frac{1}{2\Delta x}(v+c)_N^k + \frac{1}{2} c_N^k \frac{\chi_{\text{out}}}{L}$$

$$\mu = \mathcal{B}_N \frac{1}{2\Delta x}(\varrho c)_N^k (v+c)_N^k - \frac{1}{2\Delta x}(v+c)_N^k$$

$$\begin{aligned}\zeta = &-\frac{3p_N^k - 4p_N^n + p_N^{n-1}}{2\Delta t} - \frac{1}{2}(\varrho c)_N^k (v+c)_N^k \frac{3v_N^\star - 4v_{N-1}^\star + v_{N-2}^\star}{2\Delta x} \\ &- \frac{1}{2}(v+c)_N^k \frac{3p_N^k - 4p_{N-1}^k + p_{N-2}^k}{2\Delta x} - \frac{1}{2} c_N^k \chi_{\text{out}} \frac{p_N^k - p^\dagger}{L} \\ &+ \frac{1}{2\Delta x}(\varrho c)_N^k (v+c)_N^k v'_{N-1}(1-\mathcal{C}_N).\end{aligned}$$

The momentum on the cell N is corrected according to

$$(\varrho v)_N^{k+1} = \varrho_N^\star \left(1 + \frac{p'_N}{p_N^k}\right)(v_N^\star + v'_N).$$

5 Numerical experiments

The test cases presented are chosen to illustrate the capability of the semi-implicit method both at the inlet and the outlet. To explain the role of the relaxation coefficient K_p at the outlet, Eq. (12) is modified to $\mathcal{L}_1 = \alpha_p K_p(p - p^\dagger)$. Similarly, at the inlet, the coefficient α_v is introduced such that $\mathcal{L}_3 = \alpha_v K_v(v - v^\dagger)$ (see Eq. (16)).

In the following, dissipation and dispersion errors are used to evaluate the quality of the solution, when a reference solution is available. We employ the methodology proposed by Takacs [10,18]. Say that q_e and q_c are exact and computed values of a quantity q under consideration. At a given time t, the mean square error can then be defined as

$$\mathcal{E}^2 = \frac{1}{N}\sum (q_e - q_c)^2$$

where the sum extends over the N nodes of the grid. Further, we define mean values and variances of the quantities by

$$\bar{q}_e = \frac{1}{N}\sum q_e \quad , \quad \bar{q}_c = \frac{1}{N}\sum q_c$$

$$\sigma_e^2 = \frac{1}{N}\sum (q_e - \bar{q}_e)^2 \quad , \quad \sigma_c^2 = \frac{1}{N}\sum (q_c - \bar{q}_c)^2 \quad .$$

Then, the mean square error can be written as

$$\mathcal{E}^2 = \sigma_e^2 + \sigma_c^2 + (\bar{q}_e - \bar{q}_c)^2 - 2\,\text{cov}(q_e, q_c), \tag{38}$$

where $\mathrm{cov}(q_e, q_c)$ is the covariance of the two signals. The correlation coefficient between the two signals is then

$$R(q_e, q_c) = \frac{\mathrm{cov}(q_e, q_c)}{\sigma_e \sigma_c}.$$

The error (38) can further be written as

$$\mathcal{E}^2 = (\bar{q}_e - \bar{q}_c)^2 + (\sigma_e - \sigma_c)^2 + 2\sigma_e\sigma_c[1 - R(q_e, q_c)]. \tag{39}$$

The different error components can now be identified. The difference between $\bar{q}_e$ and $\bar{q}_c$ is the conservation error as the mean values of the signals express the content of the signals. The difference between σ_e and σ_c is the dissipation error as the variances express the energy of the signals with respect to their mean values. The remaining component was considered by Takacs [18] as the dispersion error, as for exact correlation between the signals, the only error that can occur is due to dissipation. This way of denoting the error does not conform completely with the now commonly used concept of the modified wave number to express dissipation and dispersion errors. In order to see the relation with the modified wave number concept, a Fourier component may be substituted into (39). This then reveals (not derived here) the rather obvious result that non-dimensional measures of dissipation and dispersion errors may be defined by

$$\check{\mathcal{E}}_{\mathrm{dissipation}} = \frac{\sigma_e - \sigma_c}{\sigma_e} \quad , \quad \check{\mathcal{E}}_{\mathrm{dispersion}} = \sqrt{1 - R(q_e, q_c)}. \tag{40}$$

For exact solutions, the error measures are zero. The error measure for dissipation becomes unity when all energy dissipates away in the computational result. The error measure for dispersion becomes unity when the correlation between exact and computational solutions disappears completely.

For the 1D test cases presented below, it will be investigated by means of a Fourier analysis if the behaviour of the dissipation and dispersion errors in Eqs. (40) is in agreement with the theoretical properties of the linear stationary filters that correspond to the inlet and outlet treatments.

In all the test cases considered in the following, the fluid is air with the specific heats ratio $\gamma = 1.4$.

5.1 Acoustic inlet oscillation

For this 1D test case, the length of the computational domain is $L = 100\ \mathrm{m}$. The inlet velocity is specified to oscillate about its mean value V, as

$$v^{\dagger}(t) = V[1 + A_v \sin(2\pi f t)],$$

where $V = 0.30886\ \mathrm{m\ s^{-1}}$, $A_v = 10^{-2}$. A_v is chosen to be sufficiently small so that an exact solution can be derived from linear acoustics. f was taken between 5 to 80 Hz so that $f/f_{\mathrm{cut-off}}$ ranges from 5 to 80. The other target values required for the boundary conditions are $\varrho^\dagger = 1.2046\ \mathrm{kg\ m^{-3}}$ and $p^\dagger = 101\ 300\ \mathrm{Pa}$. The initial conditions are

$$\begin{cases} \varrho^0 = 1.2046\ \mathrm{kg\ m^{-3}}, \\ v^0 = V\ \mathrm{m\ s^{-1}}, \\ p^0 = 101\ 300\ \mathrm{Pa}. \end{cases}$$

The simulation duration $t_f = 0.55\ \mathrm{s}$ is chosen such that no reflected wave can possibly reach the inlet before the time t_f. The mesh is regular with $N = 5\ 000$ cells. At the inlet, we take $\alpha_v = 10^4$ and $K_\varrho = 10^{-4}$ [3].

In figure 1, the role of the relaxation coefficient α_p at the outlet is shown through the total acoustic energy in the pipe, given by (linear acoustics)

$$E_a = \int_0^L \left\{ \frac{1}{2}\varrho_0 (\delta v)^2 + \frac{1}{2}\frac{(\delta p)^2}{\varrho_0 c_0^2} \right\}. \tag{41}$$

The convective CFL number is chosen as 10^{-2}. With this value, the acoustic CFL number is around 10 in the domain reached by the wave and the cut-off frequency at the outlet is around $1\mathrm{Hz}$. With $\alpha_p = 1$, the level of reflection of the monochromatic wave of frequency 20 Hz is very low, since the total acoustic energy in Eq. (41) oscillates around a constant value as soon as the acoustic wave reaches the outlet.

In figure 2, the non-reflective behaviour of the outlet is obtained even if the acoustic CFL number is significantly larger than unity, which was the main objective of the present study. Moreover, this result holds even when the acoustic energy is underestimated, due to the numerical dissipation that arises when the acoustic CFL number is very high (see the numerical results of the total acoustic energy for $\mathrm{CFL}_{v+c} = 20$ or 50 in figure 2).

Reflective conditions may be obtained by taking $\mathcal{L}_1 = \mathcal{L}_3$ in the LODI equations (11) (see *e.g.* Ref. [5]), which become then:

$$\partial_t v = 0, \ \ \partial_t p = -\varrho c \mathcal{L}_3,$$

so that, according to this approach, no pressure-velocity coupling occurs at the boundary. Another possible approach to obtain reflection at the outlet consists in setting in the LODI equations $\mathcal{L}_1 = \alpha_p K_p (p - p^\dagger)$ with $\alpha_p \gg 1$. Then, the reflection

[3] With $K_\varrho \ll 1$, the density perturbation is allowed to follow the pressure perturbation in the isentropic way. Then, the inlet condition can be interpreted as the imposition of the entropy.

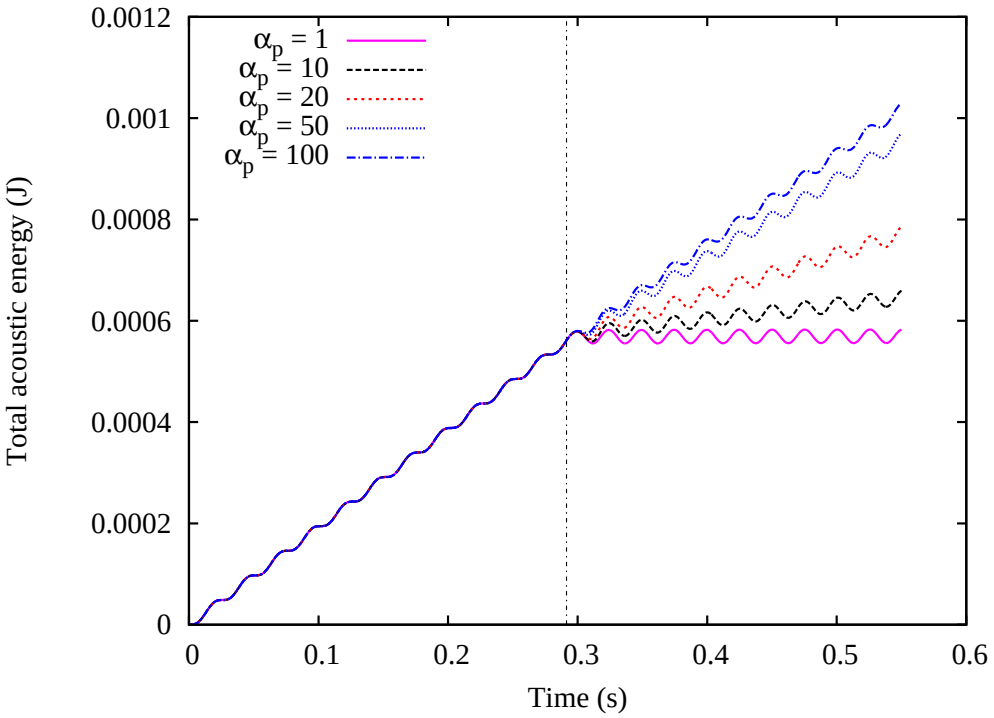


Fig. 1. Test: Acoustic inlet oscillation (*cf.* Sec. 5.1). $f = 20$ Hz, $A_v = 10^{-2}$. Time evolution of the total acoustic energy, *cf.* Eq. (41). Mach number of the mean flow: 10^{-3}; $\mathrm{CFL}_{v+c} = 10$.

coefficient becomes close to -1 (see Eq. (13)) so that the outlet becomes reflective. Notice that in this case we do not have $\partial_t v = 0$ at the outlet, and the pressure depends on the velocity, since from Eqs. (11b)-(11c),

$$\frac{1}{\varrho c}\partial_t p + \alpha_p K_p (p - p^\dagger) = \partial_t v,$$

and thus,

$$p(t) = p^\dagger + \frac{1}{\alpha_p K_p}\int_0^t \mathrm{e}^{-\varrho c \alpha_p K_p (t-s)} \partial_s v \, \mathrm{d}s,$$

under the assumptions that $\varrho c = \mathrm{const.}$ and $p(0) = p^\dagger$. Thus, using $\alpha_p \gg 1$ in $\mathcal{L}_1 = \alpha_p K_p (p - p^\dagger)$ leads to a pressure-velocity coupling on the outlet cells. In figures 3-6 are shown dispersion and dissipation errors (see Eqs. (40)) as function of time for varying frequency of the inlet oscillation and for varying acoustic CFL number. The reference solution is obtained from linear acoustics with perfect reflection at the outlet. In particular, the large error level in the reflected signal for large frequency and large acoustic CFL number is obvious. The conclusion is that for accurate simulation of the reflected wave, the time-step has to be chosen sufficiently small, with respect to the period of the oscillating signal.

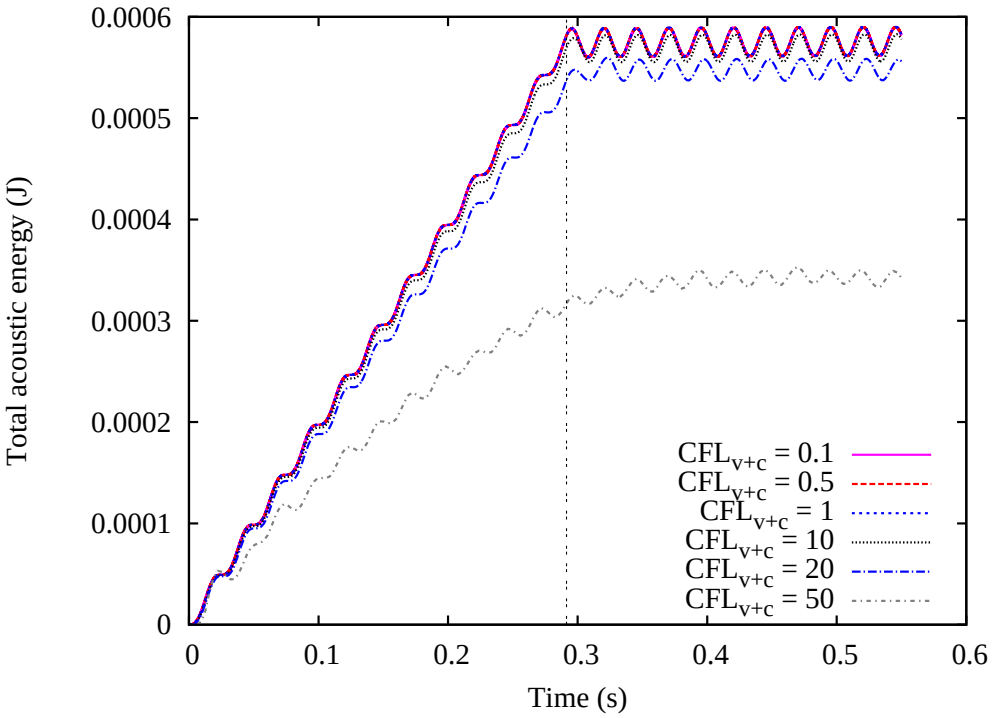


Fig. 2. Test: Acoustic inlet oscillation (*cf.* Sec. 5.1). $f = 20$ Hz, $A_v = 10^{-2}$. Time evolution of the total acoustic energy, *cf.* Eq. (41). Mach number of the mean flow: 10^{-3}; $\alpha_p = 1$.

To get insight into this issue, Eq. (A.1b) [4] is written in a first-order accurate implicit time discretization form, as

$$(\check{p} - \check{p^\dagger})^{n+1} = \frac{1}{1 + \frac{\check{\varrho}\check{c}\alpha_p \check{K}_p}{2\mathrm{M_r}}\Delta\check{t}}(\check{p} - \check{p^\dagger})^n + \frac{\check{\varrho}\check{c}\alpha_p \check{K}_p}{2\mathrm{M_r}(1 + \frac{\check{\varrho}\check{c}\alpha_p \check{K}_p}{2\mathrm{M_r}}\Delta\check{t})}\varphi^n, \tag{42}$$

where $\varphi = -{\mathrm{M_r}}^2 \check{\mathcal{L}}_3 / \check{K}_p$. Then, supposing that $\check{p}^0 = \check{p^\dagger}$, Eq. (42) yields

$$\check{p}^n = \check{p^\dagger} + \sum_{k=-\infty}^{+\infty} h_k \varphi^{n-k},$$

where

$$h_k = \begin{cases} \frac{\check{\varrho}\check{c}\alpha_p \check{K}_p \Delta\check{t}}{2\mathrm{M_r}(1+\frac{\check{\varrho}\check{c}\alpha_p \check{K}_p}{2\mathrm{M_r}}\Delta\check{t})^k} & \text{if } k = 1, 2, \ldots, n-1, \\ 0 & \text{else.} \end{cases} \tag{43}$$

The sequence (h_k) in Eq. (43) can be interpreted as the impulse response of a

[4] For equations labelled with A, see the Appendix section. The notation $\check{}$ indicates non-dimensional quantities, as defined in the Appendix section.

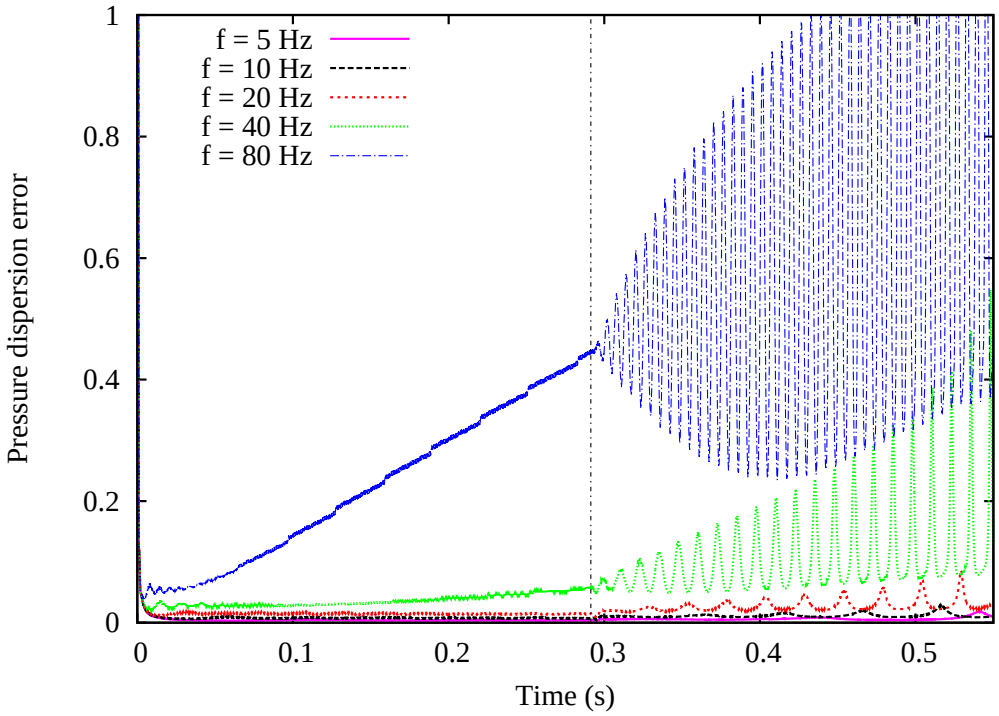


Fig. 3. Test: Acoustic inlet oscillation (*cf.* Sec. 5.1). Time evolution of the pressure dispersion error, *cf.* Eqs. (40). Mach number of the mean flow: 10^{-3} ; $\mathrm{CFL}_{v+c} = 5$; $\alpha_p = 10^3$.

discrete filter, whose transfer function is

$$\hat{h}(\check{\omega}) = \sum_{n=-\infty}^{+\infty} h_n \mathrm{e}^{-\mathrm{i}\check{\omega} n \Delta\check{t}} = \frac{\check{\varrho}\check{c}\alpha_p \check{K}_p \Delta\check{t}}{2\mathrm{M_r}[(1 + \frac{\check{\varrho}\check{c}\alpha_p \check{K}_p}{2\mathrm{M_r}}\Delta\check{t})\mathrm{e}^{\mathrm{i}\check{\omega}\Delta\check{t}} - 1]}. \tag{44}$$

The phase shift induced by the filter is obtained from Eq. (44) as

$$\arg\left(\hat{h}(\check{\omega})\right) = -\arctan\left\{\frac{\sin(\check{\omega}\Delta\check{t})}{\cos(\check{\omega}\Delta\check{t}) - \frac{1}{1+\frac{\check{\varrho}\check{c}\alpha_p \check{K}_p}{2\mathrm{M_r}}\Delta\check{t}}}\right\}. \tag{45}$$

Practically, for the values of Δt and ω considered in the present study, the phase shift induced by the outlet filter increases linearly with the time-step for a fixed frequency, and increases linearly with the frequency for a fixed time-step (see figure 7). This corresponds to the behaviour of the dispersion error observed in figures 3 and 5. On the other hand, the modulus of the outlet transfer function, related to the dissipative features of the filter, is obtained from Eq. (44) as

$$|\hat{h}(\check{\omega})| = \frac{\check{\varrho}\check{c}\alpha_p \check{K}_p \Delta\check{t}}{2\mathrm{M_r}\sqrt{\left(1 + \frac{\check{\varrho}\check{c}\alpha_p \check{K}_p}{2\mathrm{M_r}}\Delta\check{t}\right)^2 - 2\left(1 + \frac{\check{\varrho}\check{c}\alpha_p \check{K}_p}{2\mathrm{M_r}}\Delta\check{t}\right)\cos(\check{\omega}\Delta\check{t}) + 1}}.$$

Practically, for the values of Δt and ω considered in the present study, $|\hat{h}(\omega)|$ is constant and equal to 1 (not shown). Therefore, the behaviour of the dissipation er-

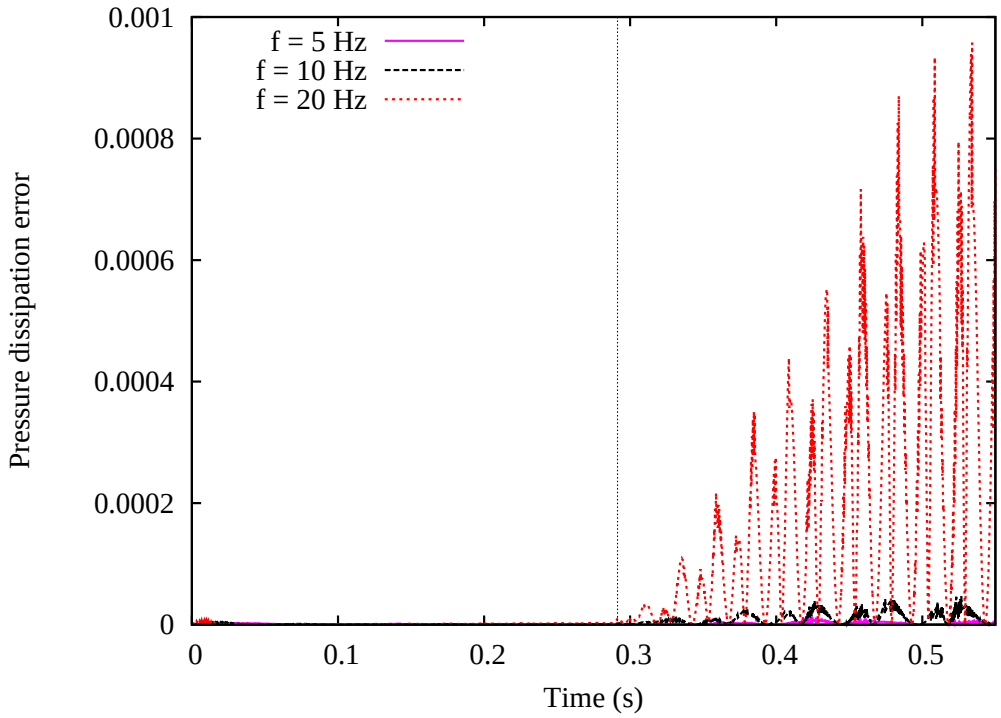


Fig. 4. Test: Acoustic inlet oscillation (*cf.* Sec. 5.1). Time evolution of the pressure dissipation error, *cf.* Eqs. (40). Mach number of the mean flow: 10^{-3} ; $\mathrm{CFL}_{v+c} = 5$; $\alpha_p = 10^3$.

ror observed in figures 4 and 6 is simply the consequence of the phase shift induced by the outlet treatment.

5.2 1-D acoustic pulse upstream propagation

Let us now consider the proposed inlet treatment with a 1D test case in which an acoustic pulse is propagating upstream in a mean flow with a Mach number of 10^{-5}. The one-meter long pipe is divided into $N = 500$ cells. Here we take $\alpha_p = 1$ and $K_\varrho = 10^{-4}$.

With $\alpha_v = 1$, the acoustic pulse leaves the computational domain without reflection (see figure 8). With $\alpha_v = 10^3$, the inlet can be considered as totally reflective (see figure 9). In figure 9, an interesting point is that the calculated reflected pulse does not coincide with the exact solution of the reflected pulse, that would be obtained if no time difference were introduced by the inlet treatment. This time difference induced by the inlet treatment can be explained by an analysis similar to the one suggested for the outlet in section 5.1. Supposing that $\check{v}(0) = \check{v}^\dagger$, the implicit time discretization of Eq. (A.1a) leads to:

$$\check{v}^n = \check{v}^\dagger + \sum_{k=-\infty}^{+\infty} h_k \phi^{n-k},$$

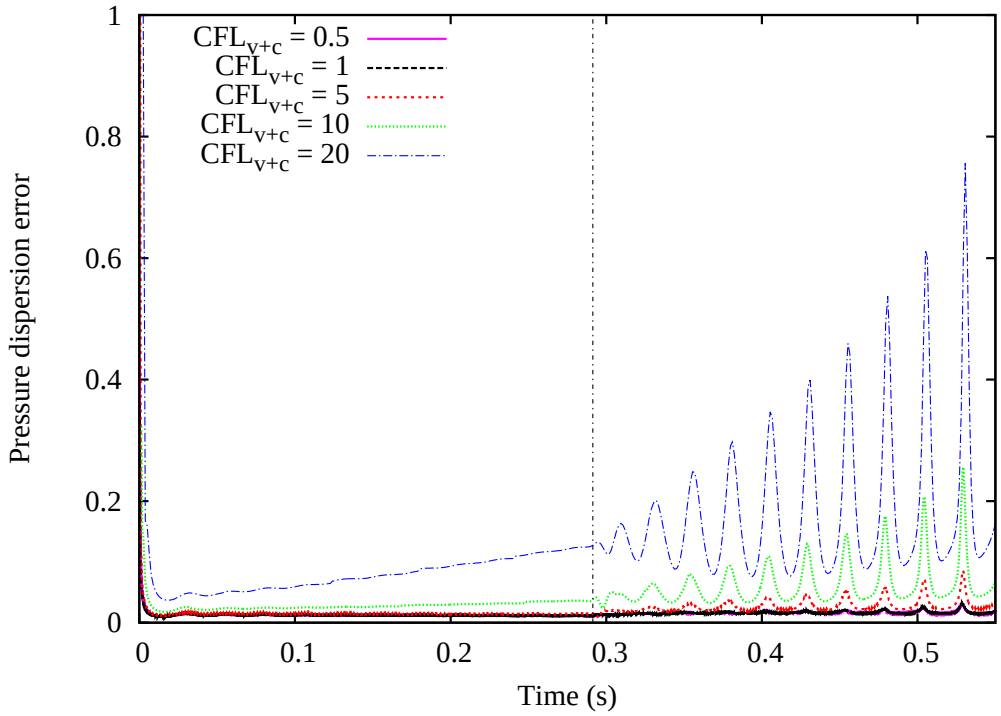


Fig. 5. Test: Acoustic inlet oscillation (*cf.* Sec. 5.1). Time evolution of the pressure dispersion error, *cf.* Eqs. (40). Mach number of the mean flow: 10^{-3} ; $f = 20$ Hz ; $\alpha_p = 10^3$. For $\mathrm{CFL}_{v+c} = 0.5$ and 1, results almost coincide.

where $\phi = \mathrm{M_r}\check{\mathcal{L}}_1/(\alpha_v \check{K}_v)$ (see Eq. (A.2a)), and

$$h_k = \begin{cases} \frac{\check{K}_v \Delta\check{t}}{2\mathrm{M_r}(1+\frac{\alpha_v \check{K}_v}{2\mathrm{M_r}}\Delta\check{t})^{k-1}} & \text{if } k = 1, 2, \ldots, n-1, \\ 0 & \text{else.} \end{cases} \tag{46}$$

The transfer function associated with the sequence in Eq. (46) is

$$\hat{h}(\check{\omega}) = \sum_{n=-\infty}^{+\infty} h_n \mathrm{e}^{-\mathrm{i}\check{\omega} n \Delta\check{t}} = \frac{\alpha_v \check{K}_v \Delta\check{t}}{2\mathrm{M_r}[(1+\frac{\alpha_v \check{K}_v}{2\mathrm{M_r}}\Delta\check{t})\mathrm{e}^{\mathrm{i}\check{\omega}\Delta\check{t}} - 1]}. \tag{47}$$

From Eq. (47), the phase shift induced by the filter at the inlet is obtained as

$$\arg\left(\hat{h}(\check{\omega})\right) = -\arctan\left\{\frac{\sin(\check{\omega}\Delta\check{t})}{\cos(\check{\omega}\Delta\check{t}) - \frac{1}{1+\frac{\alpha_v \check{K}_v}{2\mathrm{M_r}}\Delta\check{t}}}\right\}, \tag{48}$$

and the modulus of the inlet transfer function is

$$|\hat{h}(\check{\omega})| = \frac{\alpha_v \check{K}_v}{2\mathrm{M_r}\sqrt{\left(1+\frac{\alpha_v \check{K}_v}{2\mathrm{M_r}}\Delta\check{t}\right)^2 - 2\left(1+\frac{\alpha_v \check{K}_v}{2\mathrm{M_r}}\Delta\check{t}\right)\cos(\check{\omega}\Delta\check{t}) + 1}}. \tag{49}$$

In figures 10 and 11, numerical results are obtained with a constant acoustic CFL

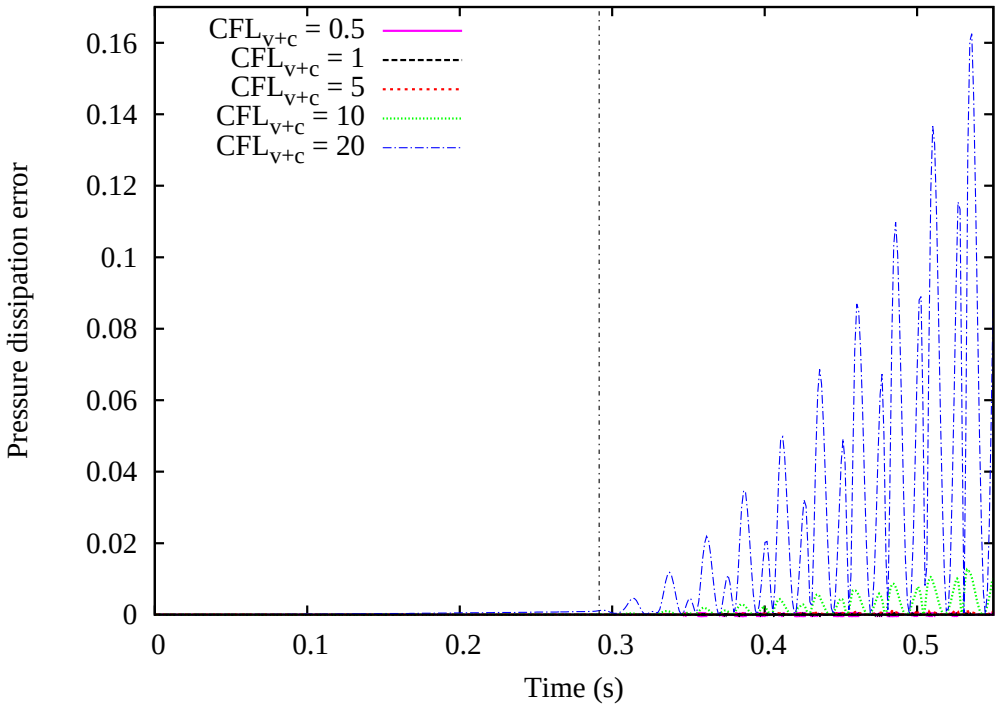


Fig. 6. Test: Acoustic inlet oscillation (*cf.* Sec. 5.1). Time evolution of the pressure dissipation error, *cf.* Eqs. (40). Mach number of the mean flow: 10^{-3} ; $f = 20$ Hz ; $\alpha_p = 10^3$. For $\mathrm{CFL}_{v+c} = 0.5$ and 1, the results coincide with the time axis.

number. As

$$\mathrm{CFL}_{v+c} = \left(1 + \frac{1}{\mathrm{M}}\right) \mathrm{CFL}_v = \left(1 + \frac{1}{\mathrm{M}}\right) \frac{v \Delta t}{\Delta x} = \left(1 + \frac{1}{\mathrm{M}}\right) \frac{\check{v} \Delta \check{t}}{\Delta \check{x}},$$

we can consider that, at low Mach number, if CFL_{v+c} is constant, then (considering that $\mathrm{M_r} = \sqrt{\gamma}\,\mathrm{M}$):

$$\Delta \check{t} \big/ \mathrm{M_r} = \text{const.} = \Phi. \tag{50}$$

For the settings considered in this study, the modulus of the inlet transfer function, written from Eqs. (49) and (50) as

$$|\hat{h}(\check{\omega})| = \frac{\alpha_v \check{K}_v}{2\mathrm{M_r}\sqrt{(1 + \frac{\alpha_v \check{K}_v}{2}\Phi)^2 - 2(1 + \frac{\alpha_v \check{K}_v}{2}\Phi)\cos(\check{\omega}\Phi\mathrm{M_r}) + 1}},$$

is practically constant for each value of the reference Mach number on the frequency band considered in figure 12, and equal to one (not shown). So, as for the outlet in section 5.1, the dissipation error shown in figure 11 is the consequence of the phase shift due to the inlet treatment.

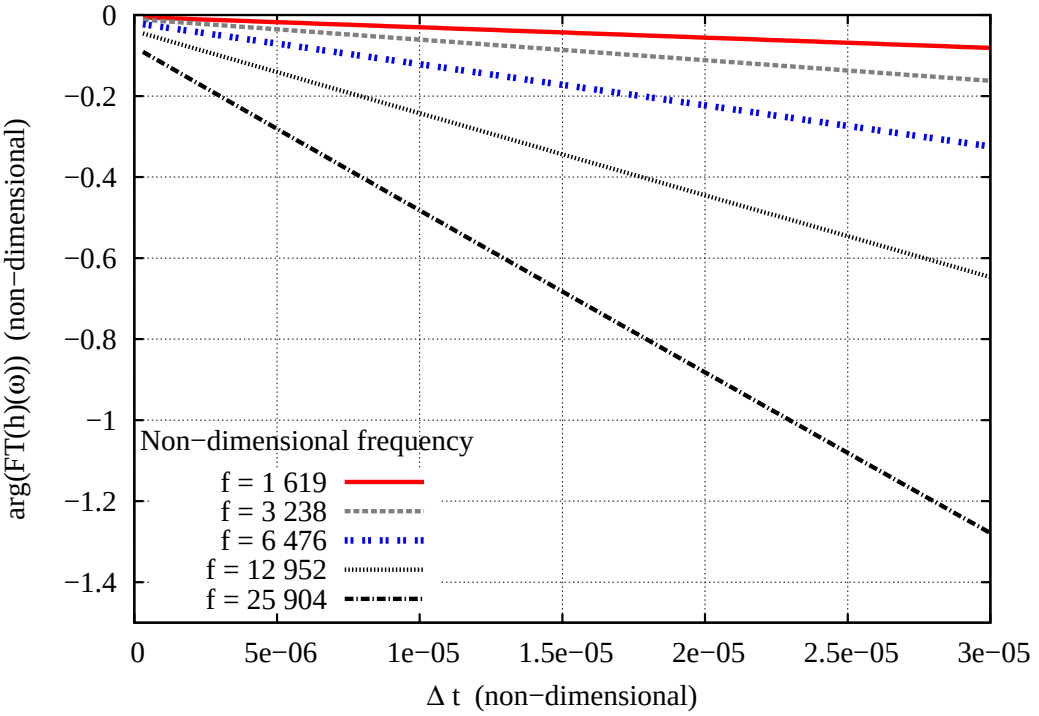


Fig. 7. Test: Acoustic inlet oscillation (*cf.* Sec. 5.1). Argument of the filter transfer function at the outlet, *cf.* Eq. (45). Mach number of the mean flow: 10^{-3} ; $\mathrm{CFL}_{v+c} = 5$; $\alpha_p = 10^3$.

From Eqs. (48) and (50), the phase shift at the inlet is written as

$$\arg\left(\hat{h}(\breve{\omega})\right) = -\arctan\left\{\frac{\sin(\breve{\omega}\Phi \mathrm{M_r})}{\cos(\breve{\omega}\Phi \mathrm{M_r}) - \frac{1}{1+\frac{\alpha_v K_v}{2}\Phi}}\right\}. \tag{51}$$

Eq. (51) with $\alpha_v = 10^3$ is illustrated in figure 12. The phase shift decreases with the Mach number for any given frequency [5] . Moreover, the phase shift level becomes practically independent of the frequency as the Mach number is the smallest considered, 10^{-7}. It is shown in figure 10 that, when the Mach number M of the background flow is small with respect to unity, the theoretical limit 0 of $\arg(\hat{h}\,(\breve{\omega}))$ (see Eq. (51)) is not achieved in practice. Moreover, the dispersion error is slightly larger for the smallest values of the background flow Mach number. The reason of these two features is that, in the previous discussion, the time discretization is solely accounted for, and not the space discretization. This is confirmed by varying the time-step, as illustrated in figure 13. Notice that the numerical results of the dispersion error are very close in figures 10 and 13 if the smallest values of M and CFL_{v+c} are considered. As shown in figure 14, the dispersion error, and hence the

[5] This is not in contradiction with the reference Mach number independency of $|R^{\mathrm{M_r}}_{\mathrm{outlet}}(\breve{\omega}_{\text{cut-off}})|$ and $\arg(R^{\mathrm{M_r}}_{\mathrm{outlet}}(\breve{\omega}_{\text{cut-off}}))$ observed in section A, since the linear filters associated with the transfer functions $\hat{h}$ and $R^{\mathrm{M_r}}_{\mathrm{outlet}}$ are different. In particular, the filter associated with $\hat{h}$ is causal and the filter associated with $R^{\mathrm{M_r}}_{\mathrm{outlet}}$ is anti-causal.

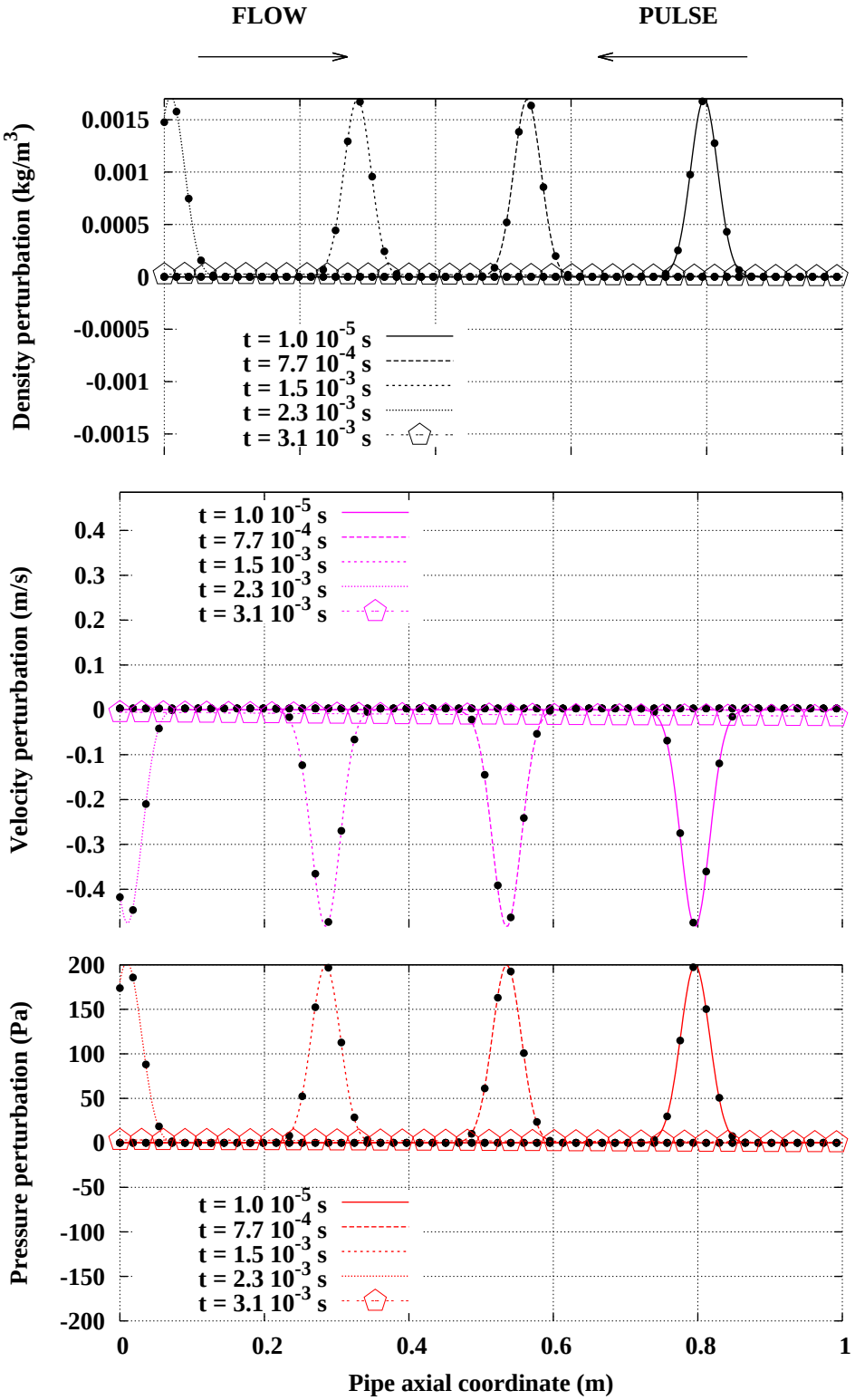


Fig. 8. Test: 1-D acoustic pulse upstream propagation (*cf.* Sec. 5.2). $\alpha_v = 1$. Mach number of the mean flow: 10^{-5}; $\mathrm{CFL}_{v+c} = 20$. Exact solution (linear acoustics): •.

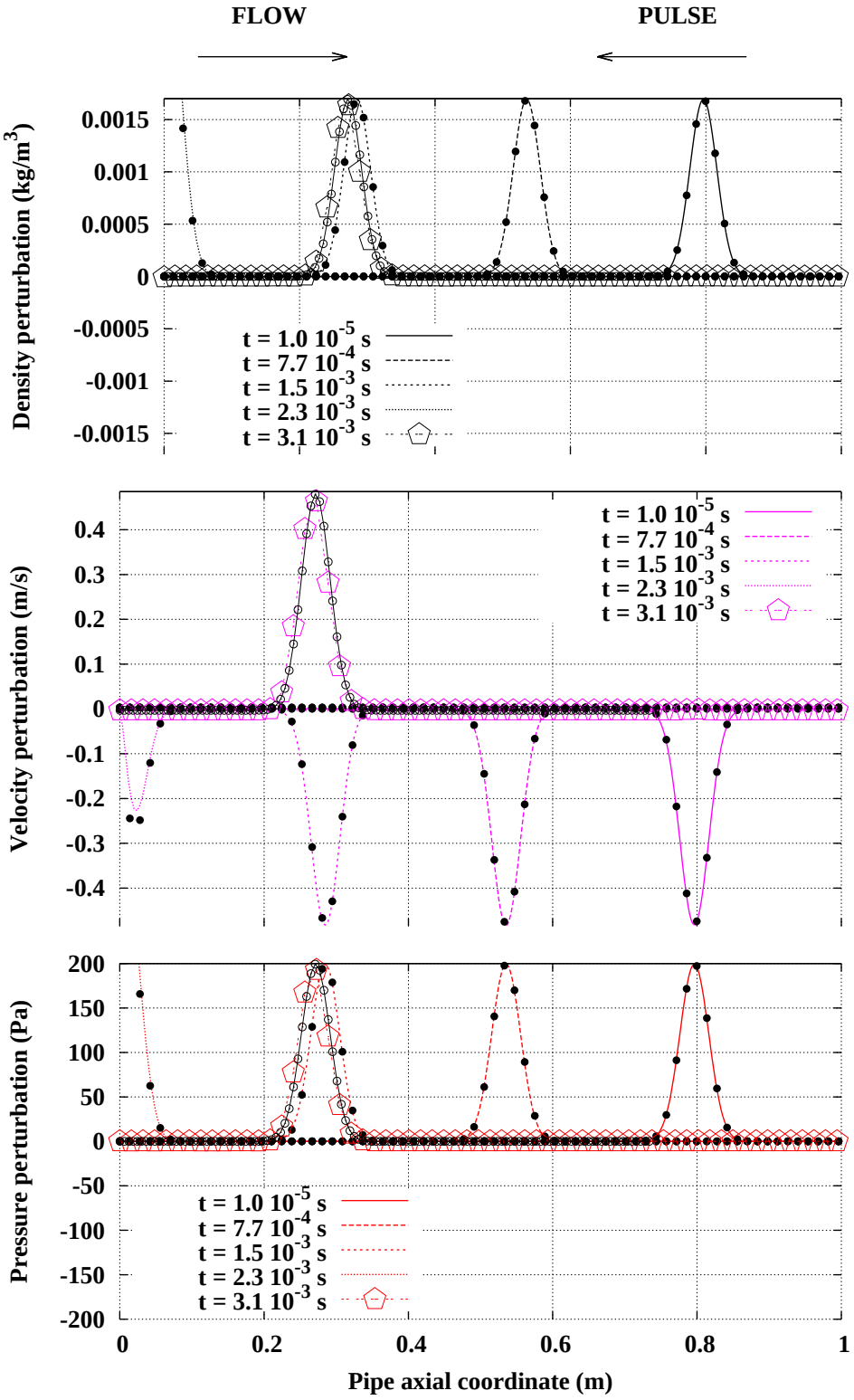


Fig. 9. Test: 1-D acoustic pulse upstream propagation (*cf.* Sec. 5.2). $\alpha_v = 10^3$. Mach number of the mean flow: 10^{-5}; $\mathrm{CFL}_{v+c} = 20$. Exact solution (linear acoustics): •. Exact solution of reflected wave: –○–.

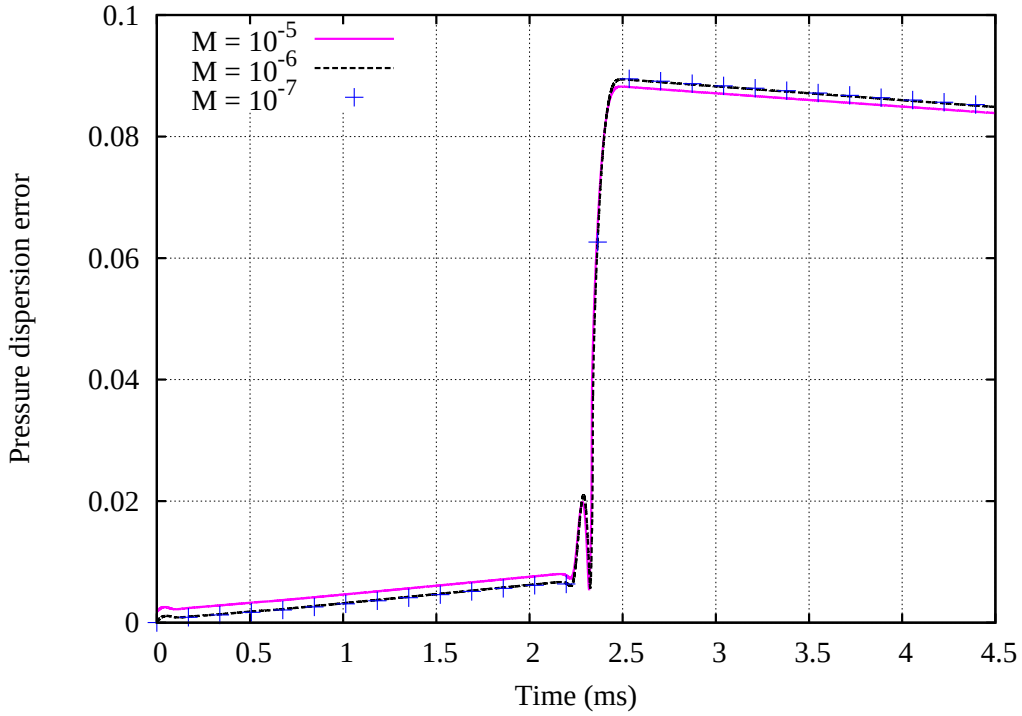


Fig. 10. Test: 1-D acoustic pulse upstream propagation (*cf.* Sec. 5.2). $\alpha_v = 10^3$, $\mathrm{CFL}_{v+c} = 5$. For $\mathrm{M} = 10^{-6}$ and 10^{-7}, results coincide.

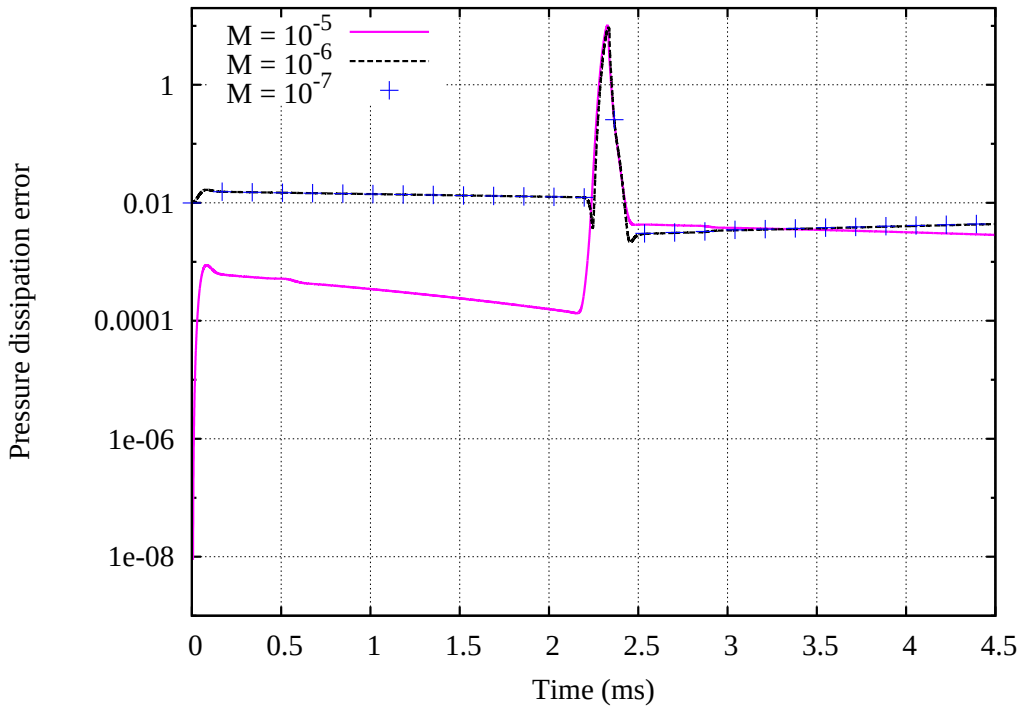


Fig. 11. Test: 1-D acoustic pulse upstream propagation (*cf.* Sec. 5.2). $\alpha_v = 10^3$, $\mathrm{CFL}_{v+c} = 5$. For $\mathrm{M} = 10^{-6}$ and 10^{-7}, results coincide.

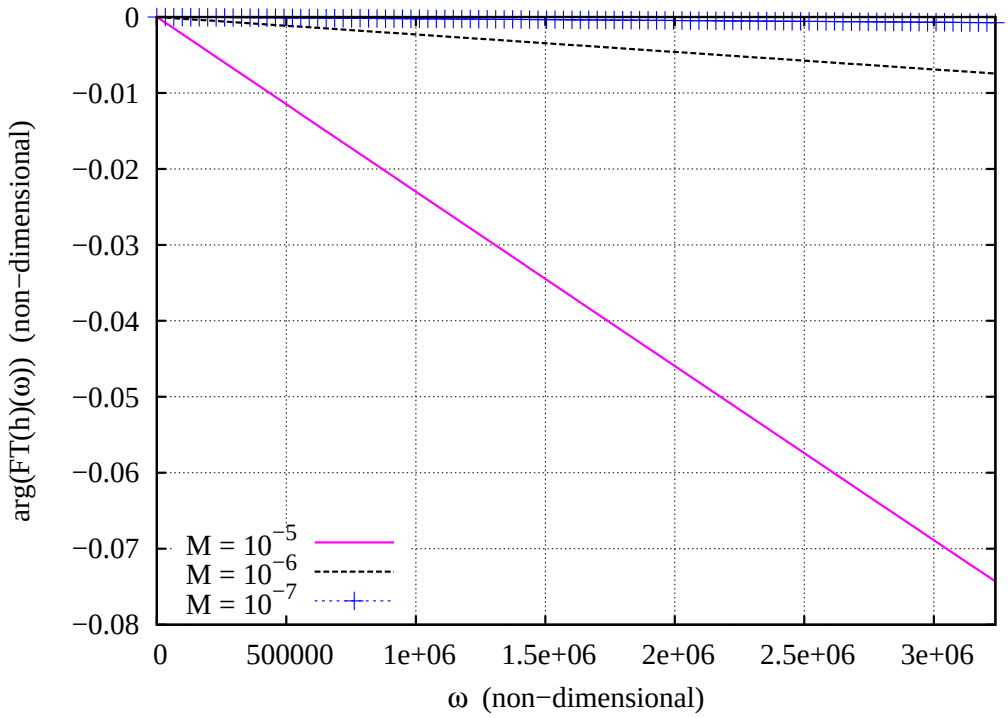


Fig. 12. Test: 1-D acoustic pulse upstream propagation (*cf.* Sec. 5.2). Argument of the filter transfer function at the inlet, *cf.* Eq. (51). $\mathrm{CFL}_{v+c} = 5$; $\alpha_v = 10^3$.

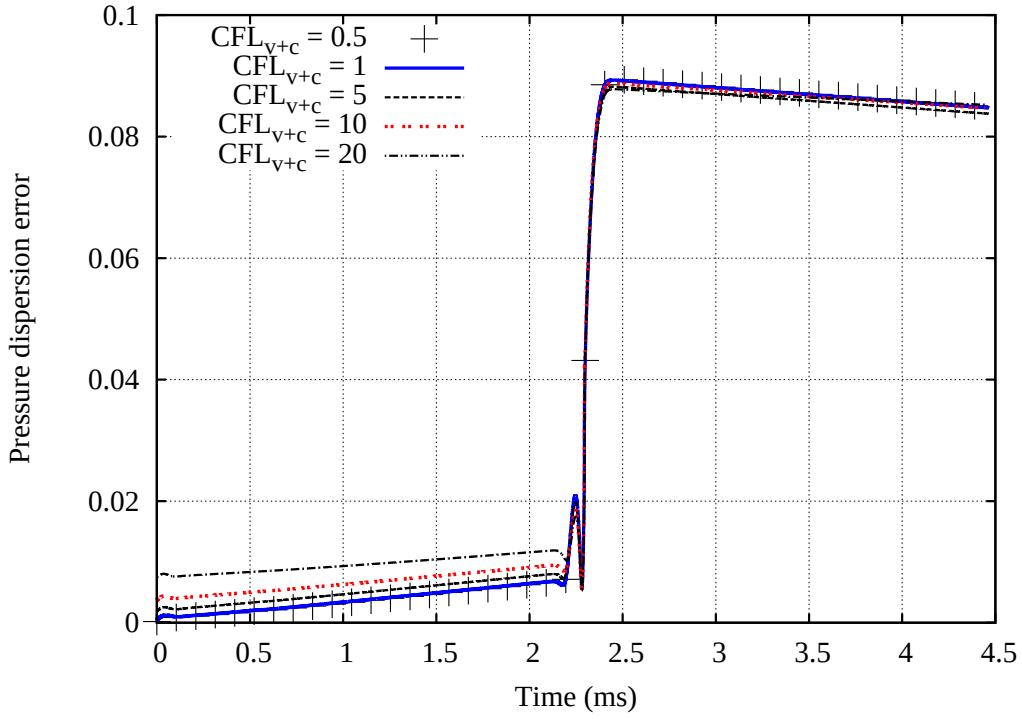


Fig. 13. Test: 1-D acoustic pulse upstream propagation (*cf.* Sec. 5.2). $\alpha_v = 10^3$, Mach number of the mean flow: 10^{-5}. For $\mathrm{CFL}_{v+c} = 0.5$ and 1, results coincide.

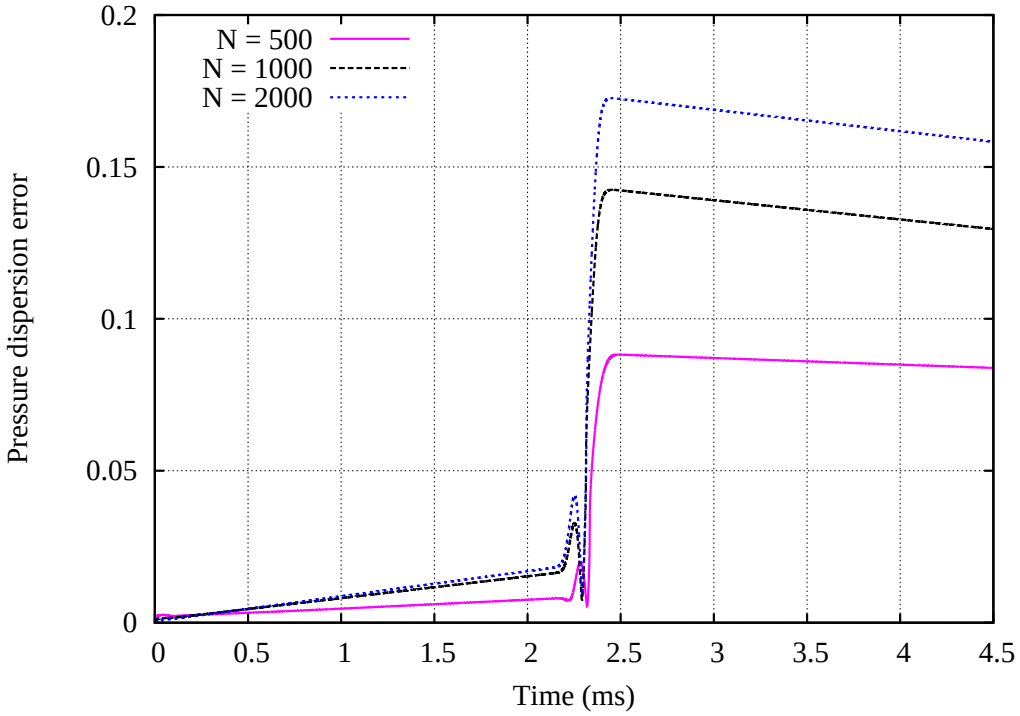


Fig. 14. Test: 1-D acoustic pulse upstream propagation (*cf.* Sec. 5.2). $\alpha_v = 10^3$, Mach number of the mean flow: 10^{-5} ; $\mathrm{CFL}_{v+c} = 5$.

phase shift due to the filter, is primarily related to the length of the boundary cells.

5.3 2-D acoustic pulse propagation

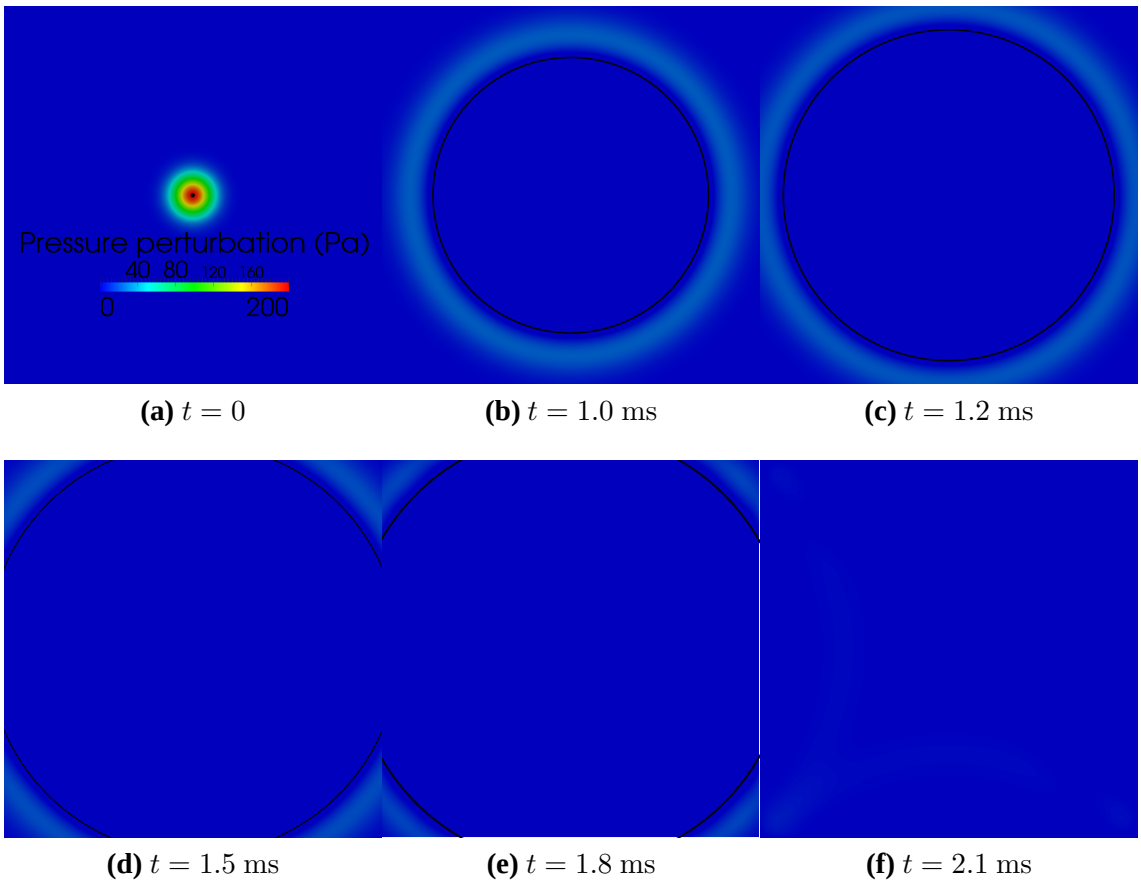
Finally, a radially propagating two-dimensional Gaussian-shaped acoustic pulse in a uniform low Mach number flow is considered. The computational domain is a square of side length 1 m, divided into 500×500 cells. The center of the pulse is located at $x_0 = 0.5$ m and $y_0 = 0.5$ m at $t = 0$. The pulse is generated at $t = 0$ by a pressure perturbation $(\delta p)^0$ and a density pertubation $(\delta \varrho)^0$ of a uniform flow which corresponds to $\varrho_0 = 1.2046$ kg m^{-3}, $u_0 = v_0 = 0.30886\ 10^{-2}$ m s^{-1} and $p_0 = 101\,300$ Pa. Entropy fluctuations are set to zero by imposing $(\delta \varrho)^0 = (\delta p)^0 / c_0^2$ where $c_0 = \sqrt{\gamma p_0 / \varrho_0}$. The initial conditions are

$$\begin{cases} \varrho^0 = \varrho_0 + (\delta \varrho)^0, \\ u^0 = u_0 \quad , \quad v^0 = v_0, \\ p^0 = p_0 + (\delta p)^0, \end{cases}$$

where the initial pressure pertubation is given by

$$(\delta p)^0 = \Delta_p \ \exp\{-\alpha[(x - x_0)^2 + (y - y_0)^2]\},$$

with $\Delta_p = 200$ Pa and $\alpha = 1/(0.05)^2 \quad \mathrm{m}^{-2}$.



(a) $t = 0$ **(b)** $t = 1.0$ ms **(c)** $t = 1.2$ ms

(d) $t = 1.5$ ms **(e)** $t = 1.8$ ms **(f)** $t = 2.1$ ms

Fig. 15. Test: 2-D acoustic pulse propagation (*cf.* Sec. 5.3). Time evolution of the pressure perturbation field (Pa) in a square of one-meter long side. Inlet: left and bottom sides of the square; outlet: right and top sides of the square. Value of the mean flow Mach number (equal in both horizontal and vertical directions): $9\ 10^{-6}$. Regular cartesian mesh, 500×500 cells. Value of the acoustic CFL number: 20. Relaxation coefficients: $\alpha_v = 1$ and $K_\varrho = 10^{-4}$ (inlet); $\alpha_p = 1$ (outlet). The black circle indicates the radial propagation of the black disc located at the center of the pulse at $t = 0$, with radial velocity $c_0 = \sqrt{\gamma p_0/\varrho_0} = 343.121$ m/s.

In figure 15, the radial velocity of the pressure perturbation is in good agreement with the reference value c_0 calculated with the density and pressure of the uniform background flow, which confirms the accuracy of the method described in section 2. No significant reflection of acoustic waves is observed, as expected with the chosen values of the reflection coefficients, since $\alpha_p = \alpha_v = 1$.

To assess the importance of the numerical dissipation due to the proposed SIMPLE-type algorithm in the results shown in figure 15, the previous simulation is reconsidered with values of reflection coefficients much larger than unity. Numerical results are shown in figure 16, right, next to the ones of Fig. 15 (f), which are displayed

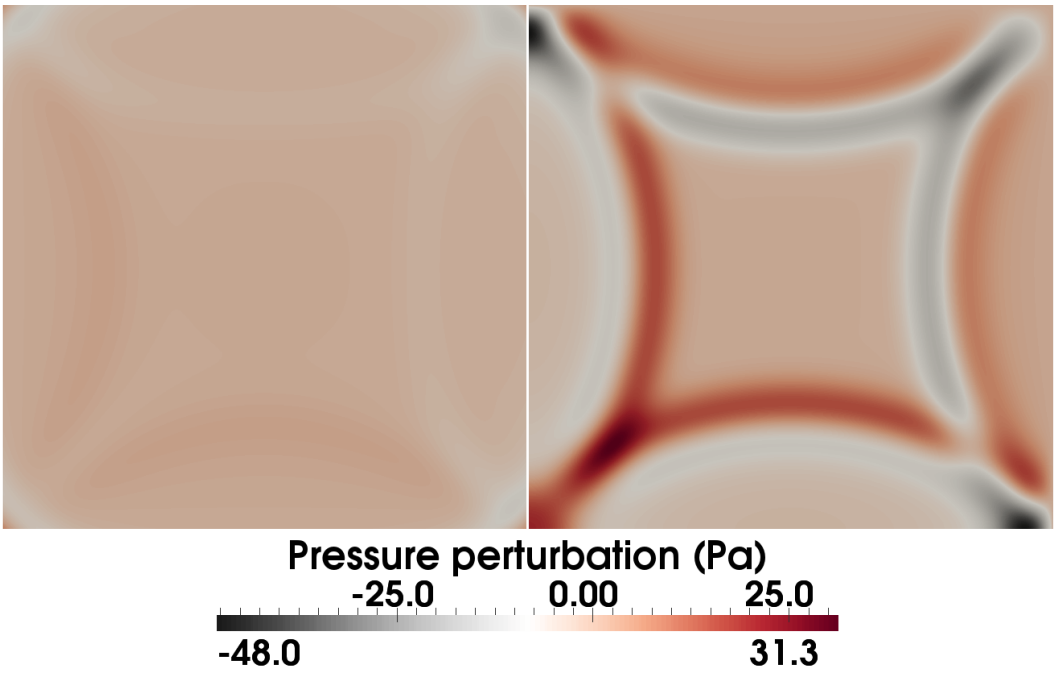


Fig. 16. Test: 2-D acoustic pulse propagation (*cf.* Sec. 5.3), $t = 2.1$ ms. Left: Computation parameters identical to those of Fig. 15 (f). Right: $\alpha_p = 10^3$ and $\alpha_v = 10^3$.

again in Fig. 16, left, with a common color map. As expected [6], it is observed that the pressure perturbation keeps its sign after reflection on the inlet line, unlike the reflected pressure perturbation on the outlet line, whose sign changes after reflection. The net visible difference between the two pressure distributions shown in Fig. 16 demonstrates that the suggested boundary treatment succeeds in this multi-dimensional test case, with an acoustic CFL number significantly larger than unity.

6 Conclusion

In this study, a partially reflective LODI-based treatment of the inlet and outlet boundaries was considered for the simulation of inviscid flows. A semi-implicit solution of the boundary equations was proposed, in combination with the algorithm used in the interior of the computational domain. The pressure-velocity coupling employed to solve the boundary equations is designed to mimic the pressure-velocity coupling used in the interior of the computational domain. The numerical experiments, carried out with a time-step that corresponds to an acoustic CFL number significantly larger than unity, show that reflective or non-reflective properties of the boundaries, well known in the framework of explicit schemes, are recovered with the proposed semi-implicit treatment.

[6] For example, see Fig. 9 bottom, for a similar feature in 1D.

A Appendix. Linear relaxation for characteristic-based boundary conditions: Low Mach number aspects

The suitability of the approach of linear relaxation form for the partially non-reflective treatment at the inlet and at the outlet is addressed in this Appendix section. Moreover, the link with classic boundary treatments for incompressible flows is established by means of an asymptotic continuous analysis, where two length scales, convective and acoustic, are distinguished (see *e.g.* Klein [4], Meister [9] or Prosser [14]).

Reference pressure p_r and density ϱ_r are introduced, along with a reference length l_r and a reference velocity v_r, which are thought of as inertial quantities. The Mach number representative of the flow is then defined as $\mathrm{M_r} = v_\mathrm{r}/\sqrt{p_\mathrm{r}/\varrho_\mathrm{r}}$. Any dimensionless quantity will be written as $\check{\cdot}$. The LODI equations (11) can now be rewritten in dimensionless form:

$$\partial_{\check{t}}\check{\varrho} + \mathrm{M_r}\frac{\check{\varrho}}{2\check{c}}(\check{\mathcal{L}}_1 + \check{\mathcal{L}}_3) + \check{\mathcal{L}}_2 = 0,$$

$$\partial_{\check{t}}\check{v} + \frac{1}{2}(\check{\mathcal{L}}_3 - \check{\mathcal{L}}_1) = 0, \tag{A.1a}$$

$$\partial_{\check{t}}\check{p} + \mathrm{M_r}\frac{\check{\varrho}\check{c}}{2}(\check{\mathcal{L}}_1 + \check{\mathcal{L}}_3) = 0, \tag{A.1b}$$

where

$$\check{\mathcal{L}}_1 = \left(\check{v} - \frac{\check{c}}{\mathrm{M_r}}\right)\left(\frac{1}{\mathrm{M_r}}\frac{1}{\check{\varrho}\check{c}}\partial_{\check{x}}\check{p} - \partial_{\check{x}}\check{v}\right), \tag{A.2a}$$

$$\check{\mathcal{L}}_2 = \check{v}\left(\partial_{\check{x}}\check{\varrho} - \frac{1}{\check{c}^2}\partial_{\check{x}}\check{p}\right), \tag{A.2b}$$

$$\check{\mathcal{L}}_3 = \left(\check{v} + \frac{\check{c}}{\mathrm{M_r}}\right)\left(\frac{1}{\mathrm{M_r}}\frac{1}{\check{\varrho}\check{c}}\partial_{\check{x}}\check{p} + \partial_{\check{x}}\check{v}\right). \tag{A.2c}$$

The outlet reflection coefficient reads now

$$R^{\mathrm{M_r}}_{\mathrm{outlet}}(\check{\omega}) = -\frac{1}{1 - \mathrm{i}\mathrm{M_r}\frac{2\check{\omega}}{\check{\varrho}\check{c}\check{K}_p}}$$

and the dimensionless cut-off frequency,

$$\check{f}_{\text{cut-off}} = \frac{(1 - M^2_{\text{max}})\check{c}_{\text{min}}}{4\mathrm{M_r}\check{L}}.$$

Thus, the modulus and argument of $R^{\mathrm{M_r}}_{\mathrm{outlet}}(\check{\omega}_{\text{cut-off}})$ are

$$|R^{\mathrm{M_r}}_{\mathrm{outlet}}(\check{\omega}_{\text{cut-off}})| = \frac{1}{\sqrt{1 + \left(\frac{2\mathrm{M_r}\check{\omega}_{\text{cut-off}}}{\check{\varrho}\check{c}\check{K}_p}\right)^2}} = \frac{1}{\sqrt{1 + \left[\frac{\pi(1-M^2_{\text{max}})\check{c}_{\text{min}}}{\check{\varrho}\check{c}\check{K}_p\check{L}}\right]^2}},$$

$$\arg(R_{\text{outlet}}^{\mathrm{M_r}}(\check{\omega}_{\text{cut-off}})) = -\pi - \arctan\left(\frac{2\mathrm{M_r}\check{\omega}_{\text{cut-off}}}{\check{\varrho}\check{c}\check{K}_p}\right)$$
$$= -\pi - \arctan\left\{\frac{\pi(1-M_{\text{max}}^2)\check{c}_{\text{min}}}{\check{\varrho}\check{c}\check{K}_p\check{L}}\right\}.$$

These expressions do not depend on the Mach number $\mathrm{M_r}$, but exhibit only a weak dependence on M_{max} in the limit $M_{\text{max}} \to 0$. In particular, the ratio of the reflected acoustic energy, fed back into the domain, to the incident acoustic energy, does not depend on the Mach number $\mathrm{M_r}$. It is easily checked that the same observation holds for the inlet treatment.

To explain the link between the charateristic-based approach previously described and a classic approach for the boundary treatment, we employ an asymptotic continuous analysis, where two length scales, convective and acoustic, are distinguished. A variable relevant to large scale acoustic fluctuations is defined as

$$\check{\xi} = \mathrm{M_r}\check{x}.$$

Then, let us suppose that the pressure variable can be expanded, when $\mathrm{M_r} \ll 1$, as

$$p(\check{x},\check{t},\mathrm{M_r}) = \sum_{n=0}^{N} {\mathrm{M_r}}^n \check{p}^{(n)}(\check{x},\check{\xi},\check{t}) + o({\mathrm{M_r}}^N) \quad , \quad N = 0,1,2$$

with similar expansions for the density $\check{\varrho}$ and the velocity $\check{v}$.

• ***Outlet***. From Eqs. (10a) and (12)-(15), the linear relaxation expression of the non-reflective condition at the outlet reads in dimensionless form

$$\check{\mathcal{L}}_1 = \frac{\pi(1-M_{\text{max}}^2)}{{\mathrm{M_r}}^2\check{\varrho}\check{L}}(\check{p} - \check{p^{\dagger}}). \tag{A.3}$$

After that the expansions in the power of the Mach number are substituted into the expressions (A.2a) and (A.3) of $\check{\mathcal{L}}_1$, one obtains:

$$\check{\mathcal{L}}_1 = \frac{\check{c}^{(0)}}{\mathrm{M_r}}\partial_{\check{x}}\check{v}^{(0)} - \check{v}^{(0)}\partial_{\check{x}}\check{v}^{(0)} + \check{c}^{(0)}(\partial_{\check{\xi}}\check{v}^{(0)} + \partial_{\check{x}}\check{v}^{(1)})$$
$$- \frac{1}{\check{\varrho}^{(0)}}(\partial_{\check{x}}\check{p}^{(2)} + \partial_{\check{\xi}}\check{p}^{(1)}) + \check{c}^{(1)}\partial_{\check{x}}\check{v}^{(0)} + o(1) \tag{A.4}$$

with

$$\check{c}^{(0)} = \sqrt{\frac{\gamma\check{p}^{(0)}}{\check{\varrho}^{(0)}}} \quad , \quad \check{c}^{(1)} = \frac{1}{2}\check{c}^{(0)}\left(\frac{\check{p}^{(1)}}{\check{p}^{(0)}} - \frac{\check{\varrho}^{(1)}}{\check{\varrho}^{(0)}}\right)$$

and, at the other hand,

$$\check{\mathcal{L}}_1 = \frac{\pi(1-M_{\text{max}}^2)}{\check{\varrho}^{(0)}\check{L}}\Bigg\{\frac{1}{{\mathrm{M_r}}^2}(\check{p}^{(0)}-\check{p^\dagger}) - \frac{1}{\mathrm{M_r}}\Big[(\check{p}^{(0)}-\check{p^\dagger})\frac{\check{\varrho}^{(1)}}{\check{\varrho}^{(0)}}+\check{p}^{(1)}\Big] + (\check{p}^{(0)}-\check{p^\dagger})\left[\left(\frac{\check{\varrho}^{(1)}}{\check{\varrho}^{(0)}}\right)^2 - \frac{\check{\varrho}^{(2)}}{\check{\varrho}^{(0)}}\right] + \check{p}^{(1)}\frac{\check{\varrho}^{(1)}}{\check{\varrho}^{(0)}} - \check{p}^{(2)} + o(1)\Bigg\}. \quad \text{(A.5)}$$

Collecting coefficients of order -2,

$$\check{p}^{(0)} = \check{p^\dagger}. \quad \text{(A.6)}$$

Let us suppose that the target pressure $\check{p^\dagger}$ is constant in time, for instance as a far-field pressure. Then, since $\mathrm{d}_{\check{t}}\check{p}^{(0)} + \gamma\check{p}^{(0)}\partial_{\check{x}}\check{v}^{(0)} = 0$ (see Ref. [4]),

$$\partial_{\check{x}}\check{v}^{(0)} = 0.$$

Finally, from Eq. (A.6) and the classical thermodynamic relation for a divariant gas:

$$\mathrm{d}\check{s} = \check{c}_V\frac{\mathrm{d}\check{p}}{\check{p}} - \check{c}_p\frac{\mathrm{d}\check{\varrho}}{\check{\varrho}}$$

one has, on isentropic assumption,

$$\partial_{\check{x}}\check{\varrho}^{(0)} = 0.$$

The previous manipulations can be summarized as follows. Suppose that the target pressure has a constant value. Then, as the representative Mach number $\mathrm{M_r}$ goes to zero, the outlet condition resulting from the linear relaxation setting, $\mathcal{L}_1 = \pi(1-M_{\text{max}}^2)(p-p^\dagger)/(\varrho L)$, leads asymptotically to the 'classical' outlet condition for the zeroth-order primitive variables, which consists of the imposition of the pressure and the extrapolation of the density and the velocity in the convective space scale.

Returning now to Eqs. (A.4) and (A.5), the order -1 yields

$$\check{p}^{(1)} = 0. \quad \text{(A.7)}$$

As the first-order pressure is identified as the acoustic one (see Ref. [4]), Eq. (A.7) corresponds to the removal of the acoustic incoming wave at the outlet. However, the proper characteristic-based non-reflective outlet condition for acoustic waves should be

$$\partial_{\check{\xi}}\check{v}^{(0)} - \frac{1}{(\check{\varrho}\check{c})^{(0)}}\partial_{\check{\xi}}\check{p}^{(1)} = 0.$$

In other words, as the representative Mach number goes to zero, the non-reflective treatment of acoustic waves degenerates asymptotically to an absorbing treatment which consists in setting the acoustic pressure to zero.

• ***Inlet***. Returning to the two length scales asymptotic expansions, since

$$\check{\mathcal{L}}_3 = \frac{\check{c}^{(0)}}{\mathrm{M_r}}\partial_{\check{x}}\check{v}^{(0)} + \check{v}^{(0)}\partial_{\check{x}}\check{v}^{(0)} + \check{c}^{(0)}(\partial_{\check{\xi}}\check{v}^{(0)} + \partial_{\check{x}}\check{v}^{(1)}) + \frac{1}{\check{\varrho}^{(0)}}(\partial_{\check{x}}\check{p}^{(2)} + \partial_{\check{\xi}}\check{p}^{(1)}) + \check{c}^{(1)}\partial_{\check{x}}\check{v}^{(0)} + o(1) \quad \text{(A.8)}$$

the identification of the expressions (A.2c) and

$$\check{\mathcal{L}}_3 = \frac{\pi(1 - M_{\max}^2)}{\mathrm{M_r}\check{L}}(\check{v} - \check{v^\dagger})$$

yields, at order -1:

$$\check{c}^{(0)}\partial_{\check{x}}\check{v}^{(0)} = \check{K}_v(\check{v}^{(0)} - \check{v^\dagger}).$$

This equation holds on an interval in which the inlet lies, at $\check{x} = 0$. On this interval,

$$\check{v}^{(0)} = \check{v^\dagger}$$

as function of $\check{x}$. Since $\check{v^\dagger}$ is supposed to be constant in time,

$$\partial_{\check{t}}\check{v}^{(0)} = 0.$$

From the zeroth-order momentum equation obtained through the convective and acoustic space scales low Mach number asymptotic analysis, one has, after separation of convective and acoustic space scales (we refer to [4,9] for details on this scales separation technique):

$$\partial_{\check{t}}\check{v}^{(0)} = -\partial_{\check{\xi}}\check{p}^{(1)} \Big/ \check{\varrho}^{(0)},$$

from which we deduce:

$$\partial_{\check{\xi}}\check{p}^{(1)} = 0.$$

Thus, the acoustic pressure is extrapolated at the inlet, with an extrapolation in the large acoustic length scale. If only the space variations of the long wavelength acoustic waves are retained in expression (A.8), the non-reflective equation $\check{\mathcal{L}}_3 = 0$ reduces at order zero to

$$\partial_{\check{\xi}}\check{v}^{(0)} + \frac{1}{(\check{\varrho}\check{c})^{(0)}}\partial_{\check{\xi}}\check{p}^{(1)} = 0.$$

Since $\partial_{\check{\xi}}\check{p}^{(1)} = 0$, the non-reflective equation of acoustic waves becomes trivial and the outcoming upstream propagating acoustic waves are set to zero. Thus, at the inlet, the filtering treatment of acoustic waves degenerates into an absorbing treatment, based on the extrapolation of the acoustic pressure. This is similar to the observations presented previously for the outlet treatment.

References

[1] T. Colonius. Modeling artificial boundary conditions for compressible flow. *Annu. Rev. Fluid Mech.*, 36:315–345, 2004.

[2] A. Kaufmann, F. Nicoud, and T. Poinsot. Flow forcing techniques for numerical simulation of combustion instabilities. *Combust. Flame*, 131:371–385, 2002.

[3] J. W. Kim, A. S. H. Lau, and N. D. Sandham. Proposed boundary conditions for gust-airfoil interaction noise. *AIAA J.*, 48(11):2705–2709, 2010.

[4] R. Klein. Semi-implicit extension of a Godunov-type scheme based on low Mach number asymptotics I: one-dimensional flow. *J. Comput. Phys.*, 121:213–237, 1995.

[5] N. Lamarque, M. Porta, F. Nicoud, and T. Poinsot. On the stability and dissipation of wall boundary conditions for compressible flows. *Int. J. Numer. Meth. Fluids*, 62(10):1134–1154, 2010.

[6] F.S. Lien and M.A. Leschziner. A general non-orthogonal collocated finite volume algorithm for turbulent flow at all speeds incorporating second-moment turbulence-transport closure, Part 1: Computational implementation. *Comput. Methods Appl. Mech. Engrg.*, 114:123–148, 1994.

[7] M.-S. Liou. A sequel to AUSM: AUSM$^+$. *J. Comput. Phys.*, 129:364–382, 1996.

[8] M.-S. Liou. A sequel to AUSM, part II: AUSM$^+$-up for all speeds. *J. Comput. Phys.*, 214:137–170, 2006.

[9] A. Meister. Asymptotic single and multiple scale expansions in the low Mach number limit. *SIAM J. Appl. Math.*, 60(1):256–271, 1999.

[10] Y. Moguen, T. Kousksou, P. Bruel, J. Vierendeels, and E. Dick. Pressure-velocity coupling allowing acoustic calculation in low Mach number flow. *J. Comput. Phys.*, 231:5522–5541, 2012.

[11] A. Pascau. Cell face velocity alternatives in a structured colocated grid for the unsteady Navier-Stokes equations. *Int. J. Numer. Meth. Fluids*, 65:812–833, 2011.

[12] T. J. Poinsot and S. K. Lele. Boundary conditions for direct simulations of compressible viscous flow. *J. Comput. Phys.*, 101:104–129, 1992.

[13] W. Polifke, C. Wall, and P. Moin. Partially reflecting and non-reflecting boundary conditions for simulation of compressible viscous flow. *J. Comput. Phys.*, 213:437–449, 2006.

[14] R. Prosser. Improved boundary conditions for the direct numerical simulation of turbulent subsonic flows. I. Inviscid flows. *J. Comput. Phys.*, 207:736–768, 2005.

[15] D. H. Rudy and J.C. Strikwerda. A nonreflecting outflow boundary condition for subsonic Navier-Stokes calculations. *J. Comput. Phys.*, 36:55–70, 1980.

[16] R. D. Sandberg and N. D. Sandham. Nonreflecting zonal characteristic boundary condition for direct numerical simulation of aerodynamic sound. *AIAA J.*, 44(2):402–405, 2006.

[17] L. Selle, F. Nicoud, and T. Poinsot. Actual impedance of nonreflecting boundary conditions: implications for computation of resonators. *AIAA J.*, 42(5):958–964, 2004.

[18] L. L. Takacs. A two-step scheme for the advection equation with minimized dissipation and dispersion errors. *Mon. Wea. Rev.*, 113:1050–1065, 1985.

[19] K. W. Thompson. Time dependent boundary conditions for hyperbolic systems. *J. Comput. Phys.*, 68:1–24, 1987.

[20] C. Wall, C. D. Pierce, and P. Moin. A semi-implicit method for resolution of acoustic waves. *J. Comput. Phys.*, 181:545–563, 2002.